Western Graduate&PostdoctoralStudies

Western University
Scholarship@Western

Electronic Thesis and Dissertation Repository

3-21-2022 4:30 PM

The Effects of a Porous Internal Lattice Design on The Articular Contact Mechanics of Radial Head Hemiarthroplasty Implants

Jessica Benitah, *The University of Western Ontario*

Supervisor: Johnson, James, *St. Josephs Hospital - Hand and Upper Limb Center*
Co-Supervisor: King, Graham, *St. Josephs Hospital - Hand and Upper Limb Center*
A thesis submitted in partial fulfillment of the requirements for the Master of Engineering Science degree in Mechanical and Materials Engineering
© Jessica Benitah 2022

Follow this and additional works at: https://ir.lib.uwo.ca/etd

 Part of the Biomechanics and Biotransport Commons, and the Mechanical Engineering Commons

Recommended Citation

Benitah, Jessica, "The Effects of a Porous Internal Lattice Design on The Articular Contact Mechanics of Radial Head Hemiarthroplasty Implants" (2022). *Electronic Thesis and Dissertation Repository*. 8435.
https://ir.lib.uwo.ca/etd/8435

This Dissertation/Thesis is brought to you for free and open access by Scholarship@Western. It has been accepted for inclusion in Electronic Thesis and Dissertation Repository by an authorized administrator of Scholarship@Western. For more information, please contact wlswadmin@uwo.ca.

Abstract

Hemiarthroplasty, where one side of a joint is replaced, is a minimally invasive procedure. It allows for the preservation of native tissue, though a significant ramification is accelerated cartilage wear when articulating with high stiffness materials that do not mimic the mechanical stiffness of the native tissue. An implant that employs a lattice design can significantly lower the stiffness of a solid structure whilst maintaining strength. This study was conducted to investigate the effect of implementing a porous internal lattice structure with a thin outer shell on the articular contact mechanics, using a radial head hemiarthroplasty. It was hypothesized that a porous internal lattice structure would reduce the effective stiffness of the implant, thus increasing hemiarthroplasty contact area and reducing contact stress relative to a solid implant. A BCC lattice was used to create the porous core of the implant surrounded by a 0.5 mm solid outer shell and was fabricated using polyamide PA2200 as the surrogate material. The lattice porosity of the radial head constructs was modified by increasing the size of the internal strut diameter (i.e., 0.4, 0.6, and 0.9 mm). A cadaveric study was performed to compare the contact mechanics of a native radial head, mid-modulus solid implant, and 65, 74, and 80%, porous implants under uniform compression over a 6-minute testing period. Contact area and stress were quantified using a Tekscan sensor interposed at the articulation. It was found that an internal lattice design can reduce articular stresses of a solid implant by approximately 40 – 65%. Future studies should further investigate the efficacy of a porous internal lattice structure using varying lattice designs, implant materials, and loading conditions to validate the effects on articular contact mechanics of hemiarthroplasty implants and ability to withstand physiologic loading conditions.

Keywords

Hemiarthroplasty, stiffness, lattice, porous, elbow, radial head, cartilage, viscoelastic, contact mechanics, contact area, contact stress

Summary for Lay Audience

Joint replacement is necessary when there is severe damage to the bones or cartilage. Hemiarthroplasty – where only one side of a joint is replaced – has become the preferred treatment method over total arthroplasty as it is cost-effective, requires less recovery time, and is minimally invasive preserving more natural tissue. A significant challenge with hemiarthroplasty is accelerated wear of cartilage when in contact with a foreign implant. Hemiarthroplasty implants are commonly made using materials much stiffer than bone or cartilage which is thought to be the reason for the rapid occurrence of cartilage damage. Lowering implant stiffness is thought to preserve cartilage health by increasing contact area and decreasing contact pressure. A lattice structure is a mesh-like structure comprised of solid beams or struts between which is empty space (pores). These structures have been shown to effectively reduce the stiffness of a solid structure while maintaining sufficient strength. Reducing the stiffness allows the implant to deform more easily and a lattice is especially advantageous in this regard as the struts can bend and absorb some of the applied force taking pressure off the cartilage on the opposing surface.

The cadaveric study presented explored changes in contact area and pressure found by using a structural lattice design – with varying strut sizes – as the internal core of a radial head hemiarthroplasty implant surrounded by a solid outer shell as compared to a solid implant and the native radial head. It was found that using a lattice structure as an implant core was effective in reducing contact stresses which could therefore reduce cartilage wear. Future studies should study the use of lattice structures in hemiarthroplasty implants by using alternative lattice designs, implant materials, and loading conditions to strengthen the validity of these findings and determine the ability to withstand a typical range of applied forces experienced during common daily activities.

Co-Authorship Statement

Chapter 1:

Jessica Benitah – wrote manuscript

James Johnson – reviewed manuscript

Graham King – reviewed manuscript

Chapter 2:

Jessica Benitah – wrote manuscript

James Johnson – reviewed manuscript

Graham King – reviewed manuscript

Chapter 3:

Jessica Benitah – study design, data collection, statistical analysis, wrote manuscript

James Johnson – study design, reviewed manuscript

Graham King – study design, reviewed manuscript

Chapter 4:

Jessica Benitah – wrote manuscript

James Johnson – study design, reviewed manuscript

Graham King – study design, reviewed manuscript

Acknowledgments

First and foremost, I would like to thank my supervisor Dr. James Johnson. Dr. Johnson is inspiringly curious and passionate about the world of biomechanics and showed continuous support and encouragement throughout this entire process. Bringing an added element of excitement every step of the way, Dr. Johnson has made this research project an absolute joy and has encouraged me to further my career in the field of biomechanical engineering. Working with Dr. Johnson has set an incredibly high standard for academic supervisors, facilitating a positive, comfortable, and encouraging working environment, and inspiring those around him. I would like to thank Dr. King as well, for volunteering his time to provide insightful commentary and a much-needed clinical perspective.

I would also like to acknowledge my lab mates Cole Fleet, David Cunningham, and Andrei Mutasa who showed me an infinite amount of support and have been so generous with their time while performing experimental testing. Finally, I would like to thank my family and friends for their uplifting words of encouragement.

I couldn't have done it without all of you!

Table of Contents

List of Figures

List of Tables

List of Abbreviations

MSK – musculoskeletal

HA – Hemiarthroplasty

OA – Osteoarthritis

RA – Rheumatoid Arthritis

THA – Total Hip Arthroplasty

TSA – Total Shoulder Arthroplasty

TKA – Total Knee Arthroplasty

DIP – Distal Interphalangeal

CMC – Carpometacarpal

PIP – Proximal Interphalangeal

DHH – Distal Humeral Hemiarthroplasty

CoCr – Cobalt Chromium

Ti – Titanium

PyC – Pyrolytic Carbon

SS – Stainless Steel

ECM – Extra Cellular Matrix

STZ – Superficial Zone

MCL – Medial Collateral Ligament

LCL – Lateral Collateral Ligament

PEEK – Poly-Ether-Ether-Ketone

HDPE – High Density Polyethylene

UHMWPE – Ultra High Molecular Weight Polyethylene

CoCrMo - Cobalt-Chrome-Molybdenum

BCC – Body-Centered Cubic

FCC – Face-Centered Cubic

KV – Kelvin

RBCC – Reinforced Body-Centered Cubic

GA – Gibson Ashby

WP – Weaire Phelan

Chapter 1

1 Introduction to Hemiarthroplasty Implants with Internal Lattice Structures

This chapter explores joint replacement, specifically the hemiarthroplasty procedure, where it is most commonly performed in the body and the associated benefits and drawbacks over total arthroplasty. This study focuses on the hemiarthroplasty of the radial head and as such covers a detailed outline of the anatomy and biomechanics of the elbow joint. Relevant literature investigating methods of improving the biomechanics of the radial head hemiarthroplasty including structure, and materials used is also discussed to provide a better understanding of how to optimize the success of the procedure with regards to overall joint health. Finally, this chapter presents the thesis rationale, hypothesis, objectives, and outline.

1.1 Joint Replacement and Hemiarthroplasty

Total arthroplasty as well has hemiarthroplasty have become leading medical treatments for a variety of musculoskeletal (MSK) health conditions[1]. A total arthroplasty refers to the replacement of the entire joint whereas a hemiarthroplasty (HA) focuses on replacing only half or parts of the joint. Hemiarthroplasty has become the preferred method of treatment to total arthroplasty in certain circumstances as it is a less invasive procedure allowing for the preservation of the native joint tissue. In addition, HA procedures can incur reduced health care costs and experience reduced recovery times[2,3].

The most common reasons for both total arthroplasty and hemiarthroplasty are MSK conditions such as osteoarthritis (OA), and rheumatoid arthritis (RA), which can cause significant damage to articular cartilage and the surrounding bone surfaces[4]. Both OA and RA are considered some of the costliest and most disabling conditions which contribute significantly to the number of annual joint replacements performed[15]. Patients with arthritis experience intense pain, swelling, and stiffness in the affected joint and in severe cases the articular cartilage is completely worn away causing the opposing bones to rub together. Without proper treatment, patients with arthritis

experience loss of function and pain in the affected joint and as such a decrease in one's quality of life. Currently, arthritis affects more than one in four adults. The condition is especially prominent in adults above the age of 65 affecting over 50% of men and 67% of women[5]. As the population grows, it is projected that people over the age of 65 are expected to double by the year 2030 thereby increasing the prevalence of these MSK conditions. Trauma, resulting in severe bone injuries where the bone has been shattered into small bone fragments that cannot be reliably repaired is another major reason for joint replacement surgery[6].

Hemiarthroplasties can be performed in many locations of the body. Most commonly, HA is performed in the knee, hip, shoulder, elbow and smaller joints of the hand and foot[1,7]. Figure 1.1 below highlights the different locations in which hemiarthroplasty procedures are commonly performed.

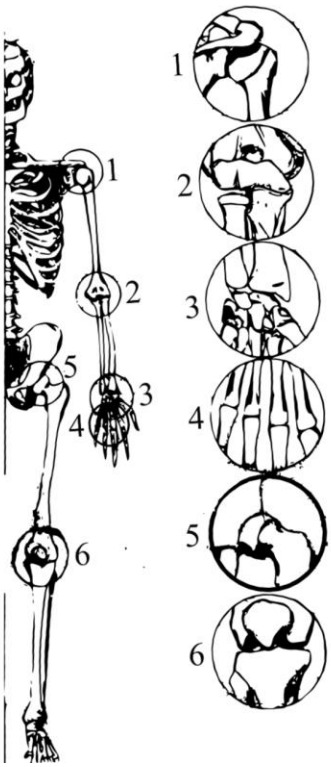

Figure 1.1 - Common Locations for Hemiarthroplasty Procedures
(1) shoulder hemiarthroplasty, (2) distal humeral hemiarthroplasty or radial head hemiarthroplasty, (3) distal radial ulnar joint, trapeziometacarpal joint, or carpometacarpal joint hemiarthroplasty, (4) proximal interphalangeal joints hemiarthroplasty, (5) hip hemiarthroplasty, and (6) knee hemiarthroplasty[7]

Among the six locations listed above, the hip is the most common location in which a hemiarthroplasty is performed. HA is typically used to treat a broken or fractured hip and to repair damage to the joint created by diseases like arthritis[4,8]. Clinicians have been leaning more towards the hemiarthroplasty procedure as opposed to a total hip arthroplasty (THA) as they typically require less surgical time, less blood loss, and a decrease chance of post-operative dislocation thereby decreasing the need for revision surgeries[8]. However, there is still some uncertainty that remains as to the benefits of a hemiarthroplasty over a THA. A randomized clinical trail was recently performed by the HEALTH Investigators, where 1495 patients with femoral neck fractures, ages 50 and older, were prescribed with a hemiarthroplasty or THA for treatment. The

trial found that neither procedure provided a clinically important outcome over the other based on the need for secondary surgeries, hip function, or overall quality of life[9]. In elderly patients specifically, who have experienced a fractured hip, hemiarthroplasty has been considered the best treatment option as it allows for immediate rehabilitation[8]. This is because hip hemiarthroplasty is often designed with a larger femoral head to decrease the likelihood of dislocation[10].

Shoulder HA is another commonly performed procedure used for the treatment of many shoulder disorders such as arthritis, humeral fractures, avascular necrosis, and capsulorrhaphy arthropathy[11]. Shoulder HA is the optimal choice when treating humeral fractures where internal fixation is not an option. However, the prevalence of the procedure has been decreasing over the years while procedures like the reverse shoulder arthroplasty have been gaining popularity[11,12]. Trofa, et al., preformed a study on the nationwide trends in total shoulder arthroplasty (TSA) and shoulder HA by analyzing and comparing patient characteristics and inpatient complications of the two procedures from 2000-2010[13]. The study reported a significant increase in the use of TSA procedures over hemiarthroplasty as it results in less need for revision surgery in the long term[13,14]. With respect to the shoulder joint, hemiarthroplasty has become secondary as a treatment modality.

Like the shoulder joint, the knee hemiarthroplasty is not as commonly performed as the total knee arthroplasty (TKA). Knee HA, however, has become the procedure of choice in the treatment of elderly patients with severe cases of OA and RA allowing for rapid post-operative rehabilitation[15]. For younger and more active patients, knee HA has become increasingly attractive as the likelihood for revision surgeries with total knee replacement is higher and the procedure allows for the preservation of more bone stock[16].

HA of the wrist is a novel procedure currently being considered for patients with severe wrist arthritis as it is thought to be able to preserve the wrists natural flexibility and range of motion. Total wrist fusion, proximal row carpectomy and total wrist arthroplasty have been most used to treat severe damage in the wrist associated with arthritis at the expense of wrist motion[17,18]. As such, midcarpal hemiarthroplasty has been under ongoing investigation as a solution to reduce patients' loss of motion. Due to the infancy of the procedure there has been a significant incidence of failure despite the procedures bone preservation capabilities[19]. In the fingers, the distal interphalangeal (DIP) joints, and the carpometacarpal (CMC) joints of the thumb are the joints in the hand most affected by diseases like OA, and RA and as such are common candidates for HA. As the conditions progress, those with DIP involvement often develop the associated symptoms in the proximal interphalangeal (PIP) joints like Bouchard nodes which over time affect the fingers range of motion and cause misalignment[20]. As such, HA of the PIP joint has become a commonly performed procedure in the treatment of diseases like OA and RA in the hands. In the past, total PIP reconstruction was reported to provide limited stability and often required revision surgery. The main source of failure has been commonly associated with excess mechanical loading placed on the bone/implant interface. HA of the PIP joint has been able to salvage more natural bone stock while providing the same benefits of a total arthroplasty[21]. However, improvements still need to be made to current PIP implants to preserve the integrity of the articulating bone.

Finally, HA in the elbow can be performed in both the radial head and the distal humerus. These two areas are of particular interest regarding elbow hemiarthroplasty however there is little information in literature regarding their outcome[22]. Radial head HA is often indicated following a fracture which occur in approximately 30% of acute elbow related injuries and are most commonly the result of a fall on an outstretched arm[23]. As shown in Figure 1.2, radial head fractures can be

classified in one of four ways: nondisplaced, displaced stable, displaced unstable, and comminuted. When the radial head is comminuted, resection or replacement is the popular choice for treatment[6]. A 2015 study investigated the post-operative function of patients who underwent radial head hemiarthroplasty and concluded that the procedure yields good short-term results providing excellent to good function, range of motion and minimal pain[24].

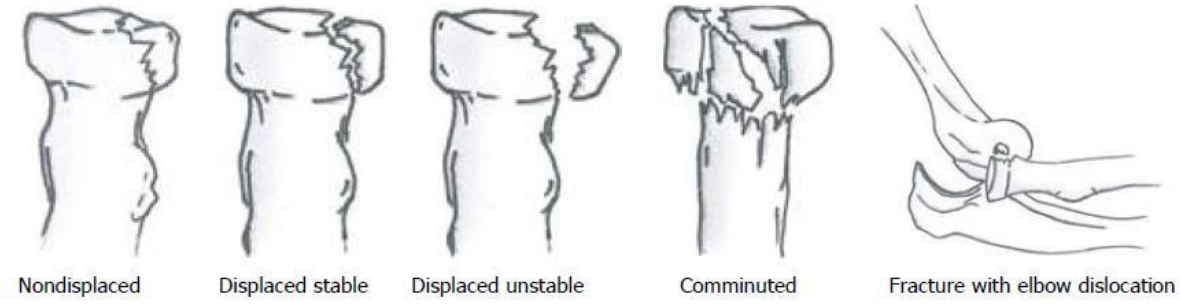

Figure 1.2 – The Different Types of Radial Head Fractures
A comminuted radial head fracture is most commonly treated with a radial head arthroplasty[25]

Distal humeral hemiarthroplasty (DHH) is another HA procedure performed in the elbow. DHH has shown to maximize the postoperative function in the ulnar and radial articulation as well as decreased surgical morbidity [22]. Current evidence regarding the outcome of the DHH is limited to case series and biomechanical data and as such the procedure remains unfamiliar to many surgeons[26].

1.2 Adverse Consequences of a Hemiarthroplasty

As described above, hemiarthroplasty has become an important option for arthritic patients who wish to preserve a higher level of function. Despite the benefits of HA over total joint replacement, the procedure can have significant drawbacks that need to be addressed to ensure the integrity of the joint is not compromised and overall joint health is preserved.

Implant shape and size is a key challenge as orthopaedic implants are not typically anatomically designed to match the native bone it is replacing or are incorrectly sized to suit the native joint. This mismatch in shape and size can lead to irregular stress distribution in the joint, accelerated cartilage wear, joint pain and implant loosening[7,27,28]. Overstuffing or understuffing of the joint are also rather concerning with regards to implant shape and size. Overstuffing the joint, where the implant is too large in length, diameter or thickness, can lead to rapid wear and erosion of the joint while understuffing the joint can lead to a irregular joint distribution and a loss of joint stability[23].

Stress shielding is another common concern in hemiarthroplasty implants where stems and bone plates made of high stiffness materials are used. Current hemiarthroplasty systems for joint replacement consist of solid metal materials including cobalt-chromium alloys (CoCr), titanium (Ti), pyrolytic carbon (PyC), and stainless steel (SS)[29]. Implant devices made with these materials pose a threat to the surrounding bone and cartilage due to a significant mismatch in material properties. Many clinically approved implants have a much higher stiffness relative to the surrounding bone tissue which causes abnormal physiological load distribution in the joint[30]. The modulus mismatch often leads to excessive movement between the implant and the bone. When these relative movements become too great the natural process of bone formation and ingrowth is drastically hindered preventing necessary implant osseointegration[31]. Bone remodeling is highly

sensitive to cyclic bone stresses and such deviations in physiologic loading can cause excess bone formation or loss; a reaction commonly referred to as stress shielding which in turn leads to implant loosening[32]. Stress shielding has been seen most commonly in HA of the hip and knee in which the articulating bone begins to resorbs and lose mass[33]. Radial head implants generate some level of stress shielding although the consequences are typically minor and non-progressive[34].

The stiffness mismatch between cancellous bone, subchondral bone, cartilage, and high stiffness implant materials are thought to also be the cause of accelerated cartilage wear at the joint interface. The modulus of cartilage is within the range of 0.5 to 0.9 MPa whereas typical radial head implants contain effective moduli within the range of 3 – 300 GPa depending on the material[35]. Regular joint movement and dynamic loading are important for the maintenance of healthy articular cartilage. However, implant devices made with high stiffness materials cause excess stress to be applied to the opposing cartilage tissue[36]. Therefore, a dramatic change in physiologic loading, be it due to immobility or the application of excess stress, can cause rapid degeneration and wear of the opposing cartilage. Accelerated cartilage wear is a common concern in the hemiarthroplasty procedure which often leads to the need for revision surgery or a replacement with a total arthroplasty[8,37–39]. Reducing cartilage wear by improving the designs of hemiarthroplasty implants is the primary focus of this thesis.

1.3 Cartilage Wear

Articular cartilage is a thin layer of specialized connective tissue found on the articular surfaces of bones that form synovial joints. This specialized tissue has a unique set of properties providing joint surfaces with minimal friction, high wear resistance, and impressive lubrication abilities which allow the tissue to withstand harsh loading conditions, protect the underlying subchondral bone and facilitate load transfer[8,36]. Articular cartilage is a viscoelastic material, meaning the tissues will respond to applied force through repeated loading progressively over time[40]. Cartilage is also a biphasic material with both a fluid and a solid phase. The biphasic nature of articular cartilage allows the joint to respond to the rapid application of pressure such that applied loads are gradually transferred to the solid phase of cartilage as the fluid phase gets pushed away into unloaded regions of the joint[41]. The fluid phase is primarily made up of water (80%) and inorganic ions such as sodium, potassium, calcium, and chloride. The solid phase is characterized by a dense extracellular matrix (ECM) which is porous and permeable[36].

Articular cartilage cells or chondrocytes in the ECM are highly specialized cells that segment articular cartilage into four zones: the superficial zone (STZ), the middle zone, the deep zone, and the calcified zone as shown in Figure 1.3[36]. The superficial zone contains tightly packed collagen fibers aligned parallel to the articular surface. The integrity of the superficial layer is vital to the protection of the other layers that make up cartilage. The superficial zone is responsible for majority of the tensile properties within cartilage which allow for the resistance of sheer, tensile and compressive forces at joint articulations[36]. The middle zone represents approximately 50% of the cartilage volume. This layer is composed of thicker collagen fibers and proteoglycans to initiate resistance to compressive forces. The deep zone is responsible for providing the greatest resistance

to compressive forces as the collagen fibers are arranged perpendicular to the articular surface. Finally, the calcified zone secures the cartilage to bone[36].

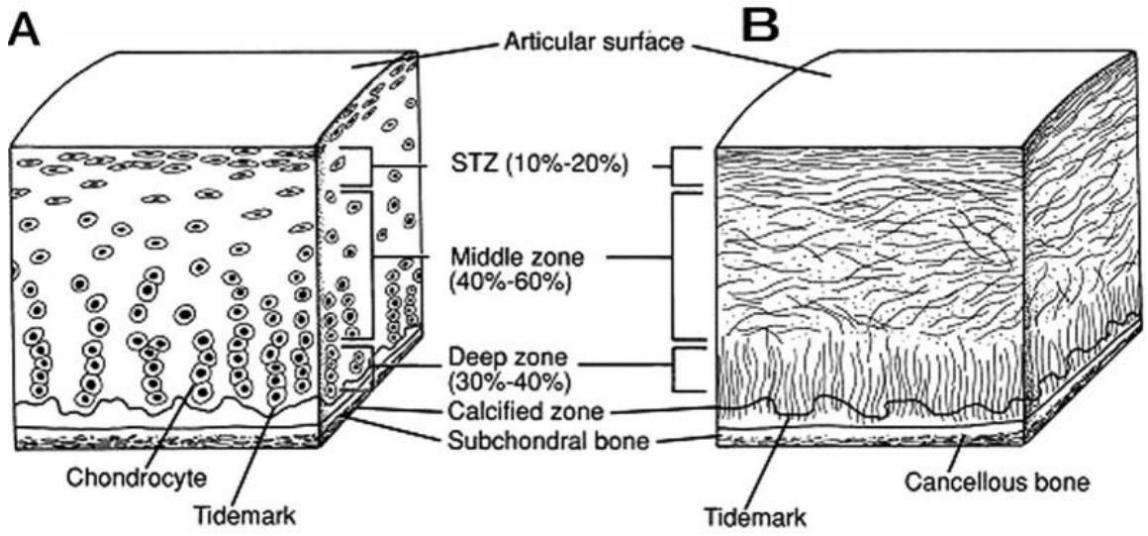

Figure 1.3 - The Multilayer Construct of Articular Cartilage[36]
(A) Chondrocyte organization (B) Cellular architecture

Cartilage will begin to wear in response to any disturbance made to the structural organization within the tissue. Damage to the superficial layer of articular cartilage inhibits the tissues' ability to bear an applied load. Osteoarthritis will form as a result of the damage to the superficial layer that will eventually progress and destroy the cartilage matrix[42]. Significant degeneration of articular cartilage can result in severe pain, swelling, and joint stiffness that can lead to long or indefinite periods of inactivity. Articular cartilage does not have blood vessels, nerves or lymphatics and therefore cannot regenerate after experiencing a significant amount of damage. HA implants pose a challenge in this regard as there is only one cartilage surface that is placed under a prolonged period of loading, resulting in an increase in the coefficient of friction at the cartilage – implant interface[8,41,39]. Therefore, protecting the integrity of articular cartilage is extremely important when considering treatment options like the hemiarthroplasty.

1.4 Elbow Anatomy

The elbow is a complex structure comprised of various components that make up an important mechanical link between the hand, wrist and shoulder. The primary role of the elbow is to allow proper positioning of the hand in space. The elbow also anchors the flexors and extensors of the hand and wrist[43]. The elbow consists of three bones, four ligaments, and five stabilizing muscles. The combined articulations of the elbow joint create one of the most stable joints in the body known as a trochleo-ginglyomoid joint able to flex and extend in the sagittal plane and rotate in pronation and supination[44]. The physiological range of motion in the elbow is typically 0-140° for flexion and extension and 0-180° for pronation and supination[45]. The elbow is a synovial joint meaning it is surrounded by an articular capsule that defines the joint cavity and is filled with synovial fluid. This fluid allows for smooth movements between the articulating surfaces of the bones[36,40,43]. To get a complete understanding of the biomechanics of the elbow, the contribution of each component of the elbow must be understood.

The elbow is one of many hinge joints in the body, comprised of three bones: the distal humerus, proximal radius, and ulna, and three articulations: the humeroulnar, radiocapitellar, and proximal radioulnar joints as shown in Figure 1.4. The distal end of the humerus is a flat in comparison to the proximal end of the humerus and is a major component of the elbow joint. On either side of the distal humerus are two protruding sections of bone called the medial and lateral epicondyles allowing for muscle fixation in the upper arm. The distal humerus also contains two round articulation areas, the trochlea and the capitellum. Just proximal of these structures are notch like areas, called fossae, which make space for the radius and ulna to permit full flexion at the joint[43]. The radius, located on the lateral side, and the ulna, located on the medial side, run parallel to each other, and make up the bones in the forearm. The proximal end of the ulna contains a large c-

shaped, trochlear notch (also called the sigmoid notch) formed by a prominent lip of bone called the coronoid process. The coronoid process articulates with the trochlea to form the humeroulnar joint. The posterior side of the humerus also contains a notch called the olecranon fossa. This notch makes space for the olecranon process of the ulna when the forearm is fully extended. The ulna contains a smooth crevasse called the radial notch forming the proximal radio-ulnar joint, a pivot joint that facilitates supination and pronation of the forearm. The proximal radius contains a small disc-shaped head that articulates with the humerus at the capitellum to form the radiocapitellar joint. The radiocapitellar joint is a convex-concave articulation where the smooth ball like capitellum sits in the concave depression of the radial head. The radial head, acts as a valgus stabilizer of the elbow, secondary to the medial collateral ligament (MCL), and provides axial stability to the forearm[43,23]. The radial head also has a significant load bearing role indicated by the trabeculae and works together with the ulnohumeral joint to prevent dislocation[23].

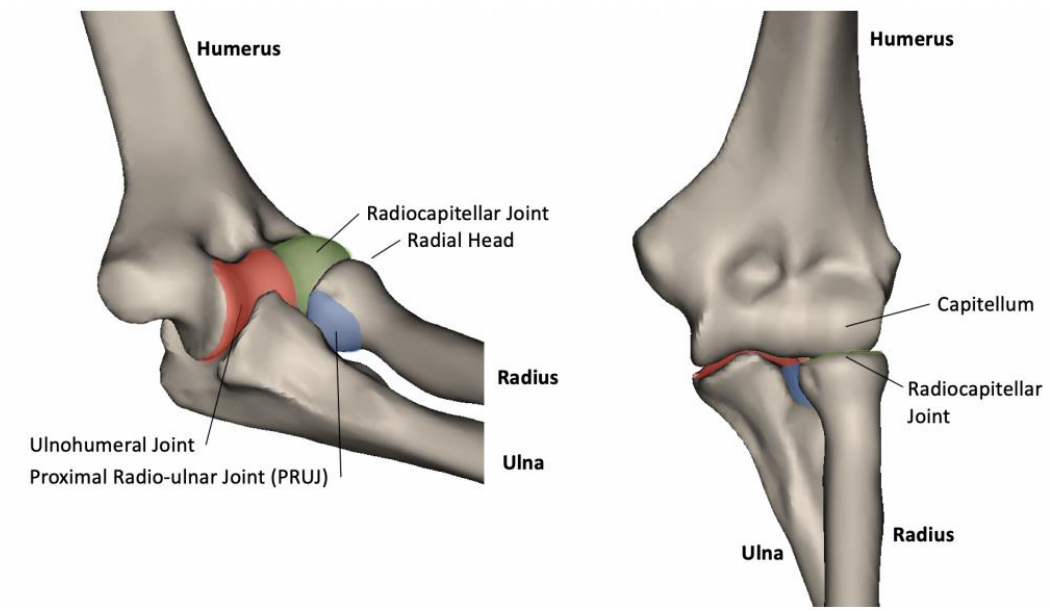

Figure 1.4 – An Anterior (left) and Posterior (right) view of the Bony Structural Anatomy of the Elbow Joint[7]
The three major articulations are highlighted in red, green, and blue representing the ulnohumeral joint, radiocapitellar joint, and radioulnar joint, respectively.

Each of the bony structures in the elbow joint are covered in articular cartilage which protects the joint from friction as the elbow moves and the bones rub together. This cartilage is soft enough to act as a shock absorber and tough enough to last a lifetime baring any complications or external damage. The distal humerus and proximal radius and ulna are also encased in a strong fibrous capsule, shown in Figure 1.5, that stabilizes the flexion and extension motions of the arm. The anterior and posterior portions of the capsule are thinner than the medial and lateral sides due to the presence of the medial collateral ligament (MCL) and lateral collateral ligament (LCL). While the elbow is in flexion, the anterior portion of the capsule is in tension and the posterior portion is in compression and vise versa. When the elbow is extended, the anterior capsule provides most of its stabilizing effects by preventing the forearm from extending past 0° [44]. The bony structures in the elbow as well as the soft tissues, tendons and ligaments are considered passive primary stabilizers to elbow function where muscles are the secondary dynamic stabilizers, controlling the compressive forces and overall function of the joint[43].

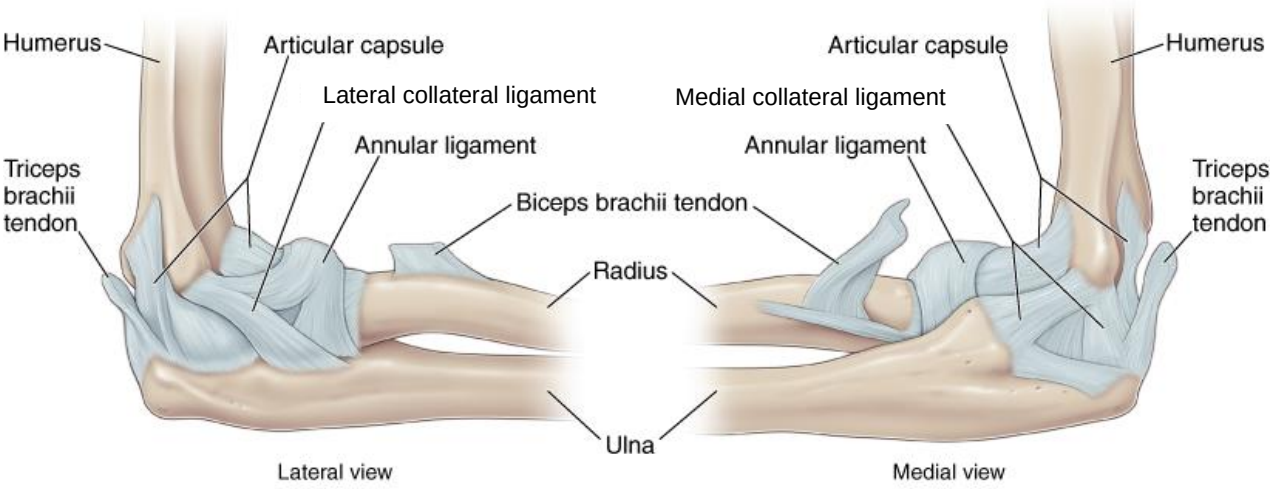

Figure 1.5- Medial and Lateral Views of the Elbow Joint Capsule and Strengthening Ligaments and Tendons[46]

1.5 Hemiarthroplasty of the Radial Head

This thesis focuses primarily on optimizing hemiarthroplasty implant compliance of the radial head because of the relative simplicity of the procedure and the ease of extending knowledge from elbow studies to hemiarthroplasties in other convex-concave joints. As such, a brief overview of previous work investigating methods to improve radial head hemiarthroplasty implant compliance is presented below.

1.5.1 Relevant Biomechanical Studies of the Radial Head Hemiarthroplasty

Radial head hemiarthroplasty complications that lead to accelerated cartilage wear are poorly understood. As such, there has been extensive literature investigating different methods of improving the contact mechanics of the radial head hemiarthroplasty. One method includes investigations on the effects of radial head implant geometry. The radiocapitellar joint has an extremely unique geometry that can vary greatly from patient to patient. As such, minor changes to radial head shape, size, and orientation may have a significant effect on the associated joint congruency and contact mechanics. In a recent study, Khayat et al used a pin-on-plate wear simulator to investigate the roles of contact geometry and implant stiffness on cartilage wear[27]. Pins of varying radii of curvature were used and as the radius of curvature decreased contact area increased. The results of this study showed a significant decrease in volumetric wear with increased contact area. This finding suggests that maximizing contact area should be a principal design target for hemiarthroplasty implants[27]. The optimization of contact area has become a rather significant variable in efforts to improve joint contact mechanics as there is a larger surface are to distribute applied loads and has been the focus of several investigations that have followed[7,27,28,47,48].

Some radial head implants today attempt to mimic the anatomic features of the native radial head however, most implants are axisymmetric or non-anatomically modeled. Such implants designs are thought to be a possible cause for accelerated cartilage wear associated with the radial head hemiarthroplasty[47]. This is due to the thought that an anatomically modeled implant would likely generate physiologic load distributions and contact mechanics similar to the native articulation[28]. Sahu et al., performed a study comparing the contact area and pressures of the native radial head to an anatomic radial head design, and a nonanatomic circular head design that is both monopolar and bipolar. This study incorporates anatomic features such as articulating dish depth, radius of curvature, and radial head shape and size to evaluate their contribution to the irregular contact mechanics seen with radial head hemiarthroplasties[28]. The anatomic radial head implants produced notably lower contact stresses than the nonanatomic models. As shown in Figure 1.6 below, these features provided an increase in the contact area at the articulation which in turn decreased the associated contact stress. Irish et al., performed a finite element study validating the results presented by Sahu et al., with the goal of determining a radial head dish depth that will optimize the contact mechanics of the prosthetic and the opposing capitellum[49]. A 2mm dish depth was found to generate the highest contact area and lowest contact pressure for metallic radial head implants with diameters within the range of 18 – 22 mm[49]. Deeper dish depths were able to optimize implant contact mechanics however stress concentrations at the edge of the implant were concerning.

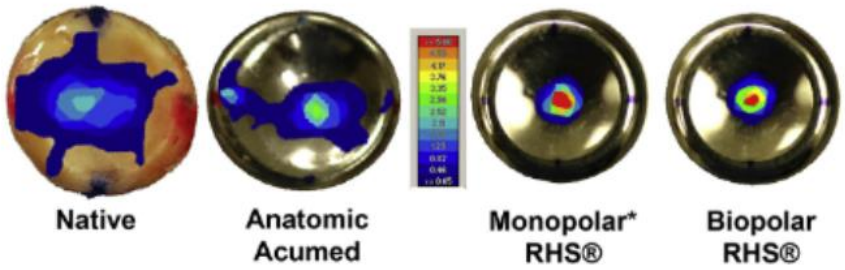

Figure 1.6 - Pressure Maps of Varying Geometric Radial Head Designs
Shown are the pressure distributions of the native radial head, anatomic, monopolar, circular, and bipolar radial head designs[28].

In contrast, A recent study performed by Langhor et al., investigated the effects of using a non-axisymmetric vs. axisymmetric implant on contact area and pressure in a finite element model[47,50]. While both implants were inferior to the native state generating higher contact stresses and lower contact areas, the axisymmetric model provided a much more consistent contact area and pressure through elbow flexion and extension and forearm rotation. A study performed by Shannon et al., compared an axisymmetric, quasi-anatomic, and patient-specific design to the native radial head and found no significant differences in implant geometry on articular contact mechanics[48].

Current prosthetic implants are modeled using high stiffness materials producing a harmful mismatch between the implant and opposing articular cartilage. This mismatch in material properties is thought to be another dominant factor contributing to the accelerated cartilage wear in hemiarthroplasty implants. In addition to geometry, further investigations have been performed on the effect of lower stiffness implant materials on articular contact mechanics. Reducing implant stiffness is thought to result in an increase in contact area and decrease in contact stress thereby reducing cartilage wear at the articulation. Khayat et al., conducted a wear study using hemispherical-tipped pins made of stainless steel, titanium, poly-ether-ether-ketone (PEEK), high density polyethylene (HDPE), and ultra high molecular weight polyethylene (UHMWPE). The pins were placed under a 27.5N load while reciprocating against cartilage plugs at a frequency of

1.2 Hz and a 10 mm stroke length for 140 minutes. Results of this study found that materials with stiffnesses within the range of 200GPa and 0.69GPa have no effect on cartilage wear[27]. Berkmortel et al., performed a similar finite element study using implant materials (i.e., CoCr, PyC, PEEK, UHMWPE, and Bionate) with a wide range of stiffness values. Radial head models of said materials were used to evaluate the contact stress and contact area under a 100N compressive load at varying angles of flexion and extension. Figure 1.7 shows the stress response of each radial head model. The green, and red regions of the figure highlight the materials that generated a significant reduction in contact stress. A clear plateau in contact stress can be seen as material modulus values surpass ~300 MPa. Despite the significant differences in stiffness for materials such as CoCr, PyC, PEEK, and UHMWPE, no significant differences in contact stress were found. These findings suggest that materials with a modulus below ~300 MPa would need to be used to achieve the desired reduction in contact stress and subsequent articular cartilage wear[7].

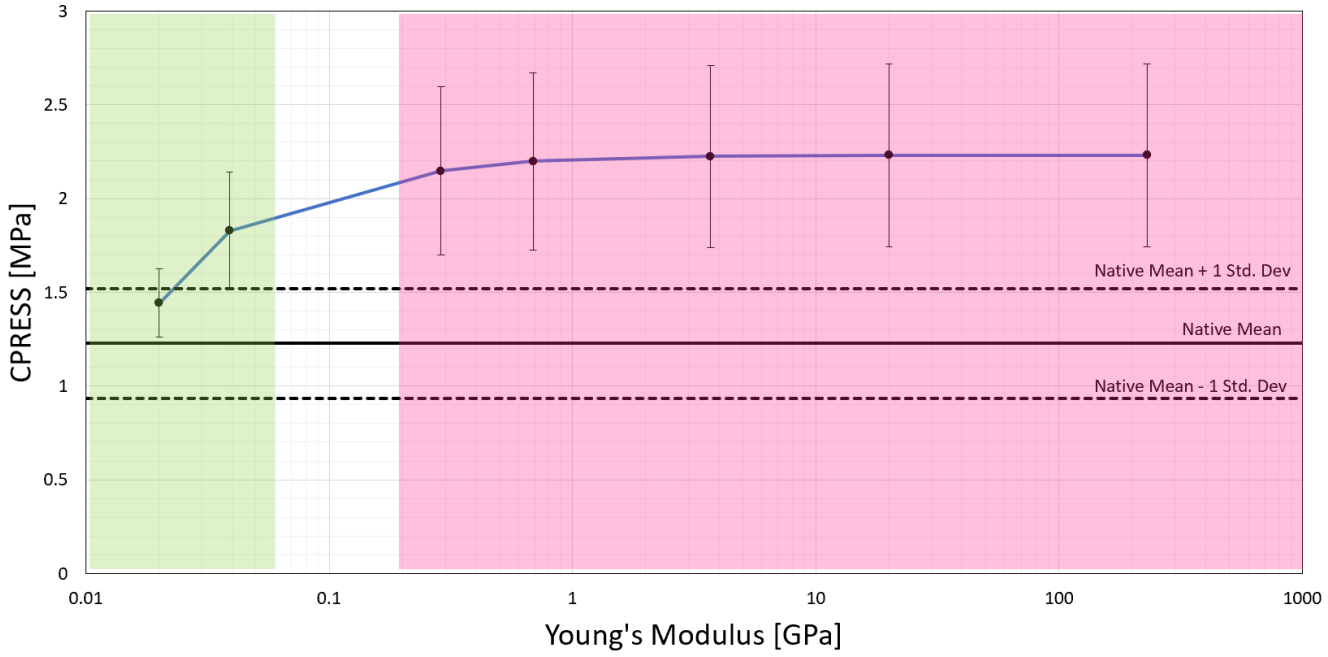

Figure 1.7 - Maximum Contact Pressure of Radial Head Models with Different Effective Moduli on a Log-Log scale as a result of the study performed by Berkmortel et al[7].
The green, white, and red highlighted regions of the graph indicate low, medium, and high modulus regions respectively.

Bionate®, (DSM Biomedical, California, USA), a medical-grade polymer, is intriguing in orthopedic research due to its durability, biostability, flexibility, toughness, and biocompatibility[3]. Dedecker et al., examined three different stiffness classes of Bionate in a study conducted to evaluate how a material with even lower effective stiffness could further reduce cartilage wear. These results were aligned with those presented by Khayat et al., and Berkmortel et al., such that as material stiffness decreased from 380 GPa to 0.02 GPa, the contact area increased, contact pressure decreased[3]. More specifically, the results of the study conducted by Dedecker et al., suggest that implant materials with a modulus within the range of 0.020 and 0.035 GPa can significantly reduce cartilage wear[3].

In an effort to further reduce implant stiffness, Berkmortel et al., conducted a finite element study on the effect of structural modifications (*viz.* total and structured hollowness) on articular contact mechanics of hemiarthroplasty implants of the radial head[7]. The proposed structures are shown in Figure 1.8. The results of this study indicated that neither totally hollow implants or partially hollow implant structures produced significant improvements with respect to contact area and contact stress. In fact, the proposed structures generated higher stresses then the solid implant. These findings were likely due to insufficient decrease in the implant's effective stiffness for some of the constructs tested, as well as the presence of stress concentrations at the edges of the implant while under compression. Furthermore, stresses within the implant increased significantly suggesting likely implant failure. In light of these findings, there is a need to investigate alternative methods of achieving low stiffness implants to improve articular contact mechanics and reduce cartilage wear.

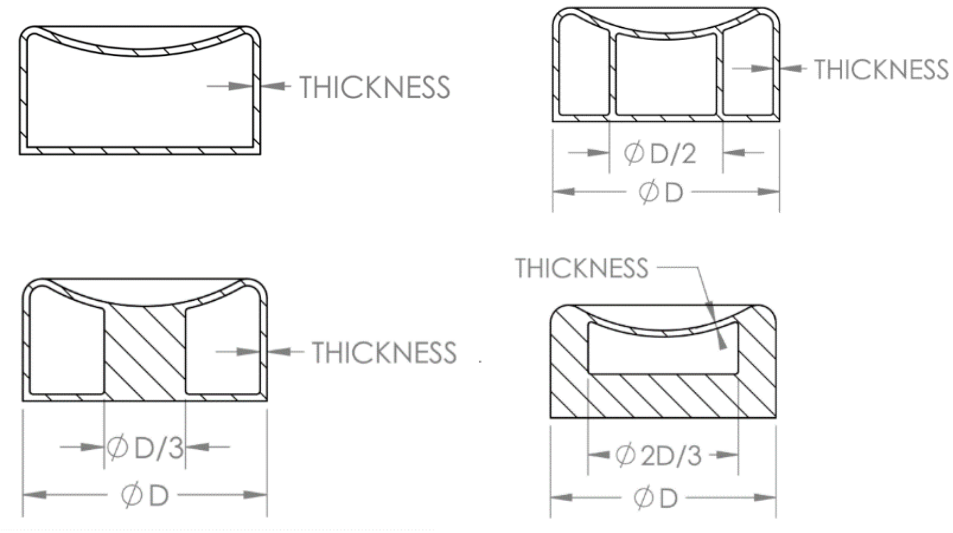

Figure 1.8 – Hollow Radial Head Implant Designs for the Investigation on the Effect of Hollowness on Implant Compliance conducted by Berkmortel et al.
The radial head implants used were axisymmetric with thickness values modified to 0.25, 0.5, 1, and 1.5mm. Thickness was uniform on each implant face. Implants of the same size were used for this study and dimensions of the hollow structures were provided relative to the diameter of the bottom face.

1.6 The Use of Porosity in Joint Replacement

The structural makeup of porous implants has been evolving since their inception 30 years ago[51]. The effect of porosity has been most explored for THA or TKA. Such studies target complications such as bone resorption, bone-implant interface micromotion, stress shielding, and implant loosening caused by high stiffness implants. To mitigate these threats many porous implants today are designed to promote bone ingrowth in which friction between the implant and the fixation surface is increased thereby increasing long-term stability[52,53]. A fully porous 3D printed femoral stem was designed by Arabnejad et al., as shown in Figure 1.7, using a multiscale material tailoring scheme. This fully porous femoral stem design is of the first targeting stress-shielding which is commonly seen with standard solid metal femoral components.

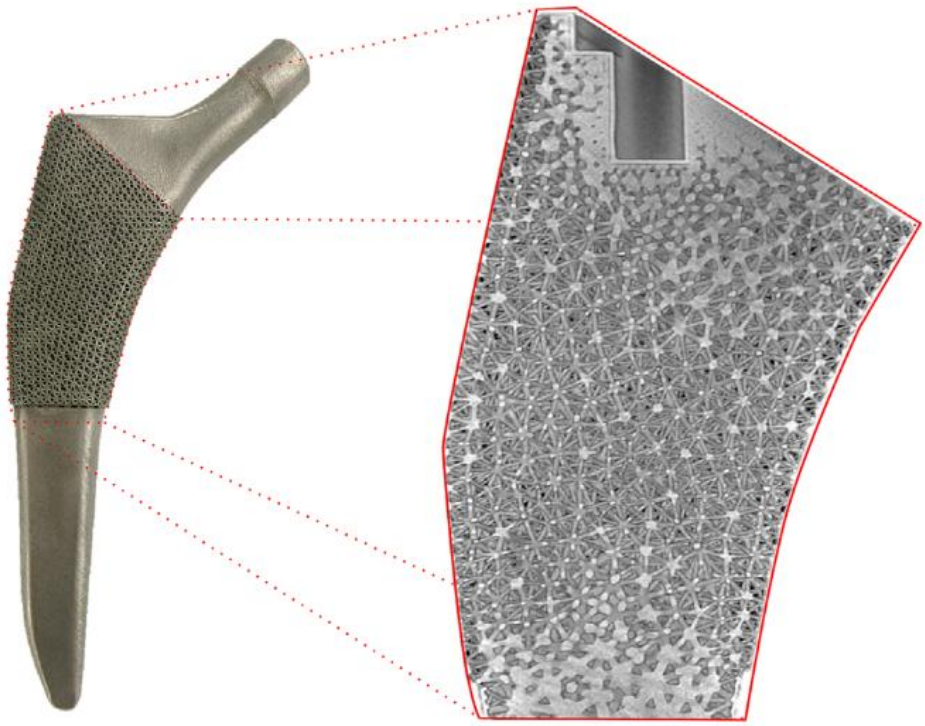

Figure 1.9 - Fully Porous 3D Femoral Stem Designed by Arabnejad et al.
The image on the left shows the manufactured implant via Selective Laser Melting and the image on the right shows the micro CT assessment of the implant lattice in the proximal region.[33]

This study shows a 75% decrease in bone loss as a result of a fully porous implant with variable stiffness[33]. The results seen from introducing porosity in the 3D printed femoral stems are promising in their ability to significantly reduce bone resorption and loosening that has been seen in the use of solid implants.

Porosity can also be introduced using cellular structures which consist of foams, honeycombs, and lattices. These structures allow for modifications to be made to the mechanical properties of a solid by altering various design parameters, and thus the volume fraction of porosity. Lattices have been recognized over foams and honeycombs as they provide a number of advantageous mechanical properties such as high stiffness and strength whilst having low mass, good energy absorption characteristics, and good thermal and acoustic insulation properties which make them suitable for various applications[54–56]. Experimental and finite element studies have shown that introducing a porous geometry via structural lattice design has been proven to tremendously reduce the effective modulus of a material – as illustrated in Figure 1.8 – and achieve similar stiffness and strength characteristics to femoral, cortical and cancellous bone[57,58,59]. Implementing lattice structures in hemiarthroplasty implants is novel it is application thus, making them an exciting new development in targeting complications such as accelerated cartilage wear as in the present work.

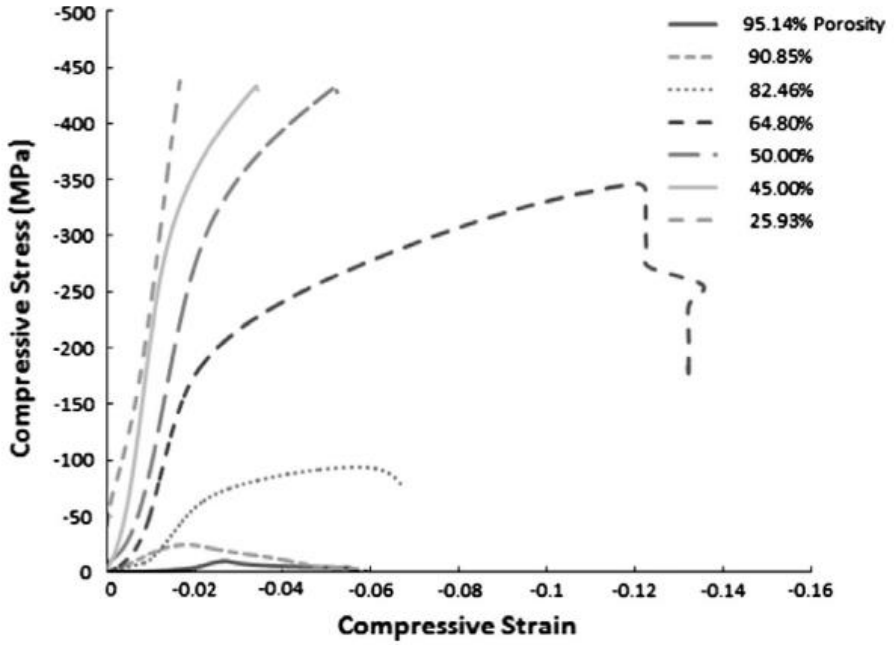

Figure 1.10 - Stress-strain relationship of Cellular Structures
Mechanical testing performed by K. Hazlehurst et al revealed that the porosities of the cellular structures range from 95%-26%. Each cellular structure was constructed from a square block of cobalt chrome molybdenum (CoCrMo) and subjected to a uniaxial compressive load.[58]

Recent literature has also focused on developing mathematical models that quantify the effect porosity has on an implant's material properties. The development of equations to predict such properties is particularly exciting, specifically with regards to Young's Modulus and Yield Strength. Important considerations in the development of these studies include equation type (linear, power, exponential, or other), implicit assumptions about the porous structure, and the valid porosity range. There is a plethora of different lattice structures that can be designed based on the type of unit cell and whether the lattice is uniform or graded in nature. A 2013 study performed a comprehensive review on such studies and concluded that there remains a lack of consideration for the specific pore structures that define these porous bodies[60]. That said, these models provide a good estimate on the expected changes in the material properties of various porous structures i.e., increasing porosity would result in a decrease in material stiffness.

In the context of this thesis, the primary concern is the preservation of articular cartilage with hemiarthroplasty implants. The mechanical properties of lattice structures have been extensively studied for use in prosthetic devices however, these structures have yet to be employed in implant design for experimental or computational assessments. To that effect, research has yet to be conducted on the articular contact mechanics of an implant which utilizes a structural lattice design and further research is paramount[60].

1.7 Thesis Rationale

Joint replacement surgery is a very common medical procedure and based on the aging population will be performed with an even higher prevalence in the future. Addressing the shortcomings in hemiarthroplasty procedures can increase the number of successful patient outcomes, reducing the number of revision surgeries needed and the tremendous financial strain on the healthcare system. The cartilage-on-cartilage interface found in synovial joints is the gold standard which technology has yet to replicate for joint replacement. The significant mismatch in material properties between articular cartilage and metal implant materials is an important reason for the accelerated cartilage wear seen with hemiarthroplasty procedures. A reduction in material stiffness can improve the contact mechanics of hemiarthroplasty implants however the magnitude of this reduction is significant. Less stiff hemiarthroplasty materials have been investigated, however their low stiffness values pose additional risks and biologic challenges that may make them unsuitable for use in vivo[61]. Mid – modulus materials such as UHMWPE, PEEK, and PyC have elastic moduli in the range of 0.7 – 20.0 GPa, which have been unsuccessful in reducing the contact stresses relative to more rigid metal implants. Hence, it is rational to postulate that structural modifications made to these polymeric materials would likely be the most efficient approach to optimize articular contact mechanics. Implementing a structural lattice design in hemiarthroplasty implants to reduce stiffness and to preserve articular cartilage health is novel and literature on the efficacy of such a technique is limited. That said, a hemiarthroplasty implant with an internal structural lattice design has the potential to optimize articular contact mechanics by generating lower stiffness values, a more deformable implant, and enabling an implant response to loading conditions that mimic those of the native articulation. As such understanding the effects of such modifications is an important area of orthopedic research.

1.8 Statement of Problem and Methodology of Solution

The stiffness mismatch between cancellous bone, subchondral bone, cartilage, and high stiffness implant materials are thought to be an important cause of accelerated cartilage wear seen with hemiarthroplasty implants. To mitigate this threat, structural modifications i.e., an internal structural lattice design will be explored to reduce implant stiffness and thereby cartilaginous stresses with the goal to improve hemiarthroplasty implant compliance and the longevity of hemiarthroplasty devices.

1.8.1 Objectives and Hypothesis

The present study will investigate the novel concept of implementing an internal lattice structure in hemiarthroplasty implants of the radial head. This will reduce the effective stiffness of the hemiarthroplasty implant with the goal of improving articular contact mechanics to produce biomechanical behaviours closer to that of the native state.

Objectives:

1. To quantify the articular contact mechanics (*viz.* contact area and contact stress) of radial head hemiarthroplasty implants with a porous internal lattice structure using experimental methods;
2. To determine a critical porosity level of the internal lattice to optimize the articular contact mechanics of the hemiarthroplasty implant.

Hypothesis:

The hypothesis of this study, is that a porous internal lattice structure would reduce the effective stiffness of the implant, thus increasing hemiarthroplasty contact area and reducing contact stress relative to a solid implant.

1.9 Thesis Overview

Chapter 2 describes the design and development of a low stiffness radial head hemiarthroplasty implant with an internal lattice structure and a thin outer shell. **Chapter 3** is a cadaveric study which investigates the contact mechanics (*viz.* contact area and stress) of the forgoing hemiarthroplasty implant models and compares them to a solid implant and the native radial head. **Chapter 4** contains general discussion, recommendations, and conclusions as per the work completed in this dissertation including future directions for this research.

1.10 References

1. Lavrenko PN, Raglis V V. *Automatic Cassette Diffusometer*. Vol 29.; 1986.

2. Pt TLU, Therapy P, Second S. Hemiarthroplasty Total Shoulder Arthroplasty Imaging of Total Joint Replacement. 2018.

3. Dedecker S. The Efficacy of Bionate as an Articulating Surface for Joint Hemiarthroplasty. 2017;(January):1-85.

4. Bleß HH, Kip M. White paper on joint replacement: Status of hip and knee arthroplasty care in Germany. *White Pap Jt Replace Status Hip Knee Arthroplast Care Ger*. 2017:1-135. doi:10.1007/978-3-662-55918-5

5. Arthritis Foundation. Arthritis by the Numbers. *Arthritis Found*. 2019:1-70. https://www.arthritis.org/getmedia/e1256607-fa87-4593-aa8a-8db4f291072a/2019-abtn-final-march-2019.pdf.

6. Pappas N, Bernstein J. Fractures in brief: Radial head fractures. *Clin Orthop Relat Res*. 2010;468(3):914-916. doi:10.1007/s11999-009-1183-1

7. Berkmortel C. Lower Stiffness Orthopaedic Implants for Hemiarthroplasty. 2020:130.

8. Lizhang J, Fisher J, Jin Z, Burton A, Williams S. The effect of contact stress on cartilage friction, deformation and wear. *Proc Inst Mech Eng Part H J Eng Med*. 2011;225(5):461-475. doi:10.1177/2041303310392626

9. Einhorn TA, Guy- G, Schemitsch EH, et al. new england journal. 2019:2199-2208. doi:10.1056/NEJMoa1906190

10. Robertson GAJ, Wood AM, Wood AM. Hip hemi-arthroplasty for neck of femur fracture :

What is the current evidence ? 2018;9(11):235-244. doi:10.5312/wjo.v9.i11.235

11. Jr DJH, Hsu JE, Iii FAM. Primary Shoulder Hemiarthroplasty : What Can Be Learned From 359 Cases That Were Surgically Revised ? 2018:1031-1040. doi:10.1007/s11999.0000000000000167

12. Wagner ER, Farley KX, Higgins I, Wilson JM, Daly CA, Gottschalk MB. The incidence of shoulder arthroplasty : rise and future projections compared with hip and knee arthroplasty. *J Shoulder Elb Surg*. 2020;29(12):2601-2609. doi:10.1016/j.jse.2020.03.049

13. Trofa D, Rajaee SS, Smith EL. Nationwide Trends in Total Shoulder Arthroplasty and Hemiarthroplasty for Osteoarthritis. 2014;(April):166-172.

14. Bekerom MPJ Van Den, Geervliet PC, Somford MP, Den MPJ Van. Original Article Total shoulder arthroplasty versus hemiarthroplasty for glenohumeral arthritis : A systematic review of the literature at long-term follow-up. 2013;7(3):3-8. doi:10.4103/0973-6042.118915

15. Gezeral OS. Prosthesis arthritis toronto,. :244-255.

16. Mccann LÃ, Ingham E, Jin Z, Fisher J. An investigation of the effect of conformity of knee hemiarthroplasty designs on contact stress , friction and degeneration of articular cartilage : A tribological study. 2009;42:1326-1331. doi:10.1016/j.jbiomech.2009.03.028

17. Vance MC, Wolfe SW, Packer G, Tan D, Crisco JJT, Ph D. Midcarpal Hemiarthroplasty for Wrist Arthritis : Rationale and Early Results. 2012;1(212):61-67.

18. Anneberg M, Packer G, Crisco JJ, Wolfe S. Four-Year Outcomes of Midcarpal Hemiarthroplasty for Wrist Arthritis. *J Hand Surg Am*. 2017;42(11):894-903.

doi:10.1016/j.jhsa.2017.07.029

19. Jr EGH, Lum Z, Bamberger HB, Trzeciak MA. Failure of Wrist Hemiarthroplasty. 2017. doi:10.1177/1558944716668836

20. Rticle CRA, Beasley J. FOR Osteoarthritis and Rheumatoid Arthritis : Conservative Therapeutic Management. *J Hand Ther*. 2012;25(2):163-172. doi:10.1016/j.jht.2011.11.001

21. Pettersson K, Amilon A, Rizzo M. Pyrolytic Carbon Hemiarthroplasty in the Management of Proximal Interphalangeal Joint Arthritis. *J Hand Surg Am*. 2015;40(3):462-468. doi:10.1016/j.jhsa.2014.12.016

22. Hohman DW, Nodzo SR, Qvick LM, Duquin TR, Paterson PP. Hemiarthroplasty of the distal humerus for acute and chronic complex intra-articular injuries. *J Shoulder Elb Surg*. 2014;23(2):265-272. doi:10.1016/j.jse.2013.05.007

23. Stuffmann E, Baratz ME. Radial Head Implant Arthroplasty. *YJHSU*. 2009;34(4):745-754. doi:10.1016/j.jhsa.2009.01.027

24. Estrada-Malacón CA, Pérez-Valtierra M, Torres-Zavala A, Fonseca-Bernal M. Hemiartroplastía de cúpula radial en pacientes con fractura tipo III y IV según Mason Johnston. *Acta ortopédica Mex*. 2015;29(3):148-154.

25. Kodde IF, Kaas L, Flipsen M, Bekerom MPJ Van Den, Eygendaal D. Current concepts in the management of radial head fractures. 2015;6(11):954-960. doi:10.5312/wjo.v6.i11.954

26. Phadnis J, Watts AC, Bain GI. Elbow hemiarthroplasty for the management of distal humeral fractures: current technique, indications and results. *Shoulder Elb*. 2016;8(3):171-

183. doi:10.1177/1758573216640210

27. Khayat A. Effect of Hemiarthroplasty Implant Contact Geometry and Material on Early Cartilage Wear. 2015;(October):1-102.

28. Sahu D, Holmes DM, Fitzsimmons JS, et al. Influence of radial head prosthetic design on radiocapitellar joint contact mechanics. *J Shoulder Elb Surg*. 2014;23(4):456-462. doi:10.1016/j.jse.2013.11.028

29. Dumas M, Terriault P, Brailovski V. Modelling and characterization of a porosity graded lattice structure for additively manufactured biomaterials. *Mater Des*. 2017;121:383-392. doi:10.1016/j.matdes.2017.02.021

30. Disc I, Ligament AC, Tis- B, Bone C, Remodeling B. Learn more about Stress Shielding Responses of Musculoskeletal Tissues to Disuse and Remobilization. 2014.

31. Krishna BV, Bose S, Bandyopadhyay A. Low stiffness porous Ti structures for load-bearing implants. *Acta Biomater*. 2007;3(6):997-1006. doi:10.1016/j.actbio.2007.03.008

32. Matassi F, Botti A, Sirleo L, Carulli C, Innocenti M. Porous metal for orthopedics implants. *Clin Cases Miner Bone Metab*. 2013;10(2):111-115. doi:10.11138/ccmbm/2013.10.2.111

33. Arabnejad S, Johnston B, Tanzer M, Pasini D. Fully porous 3D printed titanium femoral stem to reduce stress-shielding following total hip arthroplasty. *J Orthop Res*. 2017;35(8):1774-1783. doi:10.1002/jor.23445

34. Chanlalit C, Shukla DR, Fitzsimmons JS, An KN, O'Driscoll SW. Stress Shielding Around Radial Head Prostheses. *J Hand Surg Am*. 2012;37(10):2118-2125.

doi:10.1016/J.JHSA.2012.06.020

35. Jin H, Lewis JL. Determination of Poisson's Ratio of Articular Cartilage by Indentation Using Different-Sized Indenters. *J Biomech Eng*. 2004;126(2):138-145. doi:10.1115/1.1688772

36. Sophia Fox AJ, Bedi A, Rodeo SA. The basic science of articular cartilage: Structure, composition, and function. *Sports Health*. 2009;1(6):461-468. doi:10.1177/1941738109350438

37. Cruess RL, Kwok DC, Duc PN, Lecavalier MA, Dang GT. The response of articular cartilage to weight-bearing against metal. A study of hemiarthroplasty of the hip in the dog. *J Bone Jt Surg - Ser B*. 1984;66(4):592-597. doi:10.1302/0301-620x.66b4.6204988

38. Chan SMT, Neu CP, Komvopoulos K, Reddi AH, Di Cesare PE. Friction and wear of hemiarthroplasty biomaterials in reciprocating sliding contact with articular cartilage. *J Tribol*. 2011;133(4). doi:10.1115/1.4004760

39. Schwartz CJ, Bahadur S. Investigation of articular cartilage and counterface compliance in multi-directional sliding as in orthopedic implants. 2007;262:1315-1320. doi:10.1016/j.wear.2007.01.007

40. Lawless BM, Sadeghi H, Temple DK, Dhaliwal H, Espino DM, Hukins DWL. Viscoelasticity of articular cartilage: Analysing the effect of induced stress and the restraint of bone in a dynamic environment. *J Mech Behav Biomed Mater*. 2017;75(May):293-301. doi:10.1016/j.jmbbm.2017.07.040

41. Katta J, Jin Z, Ingham E, Fisher J. Biotribology of articular cartilage-A review of the

recent advances. *Med Eng Phys*. 2008;30(10):1349-1363. doi:10.1016/j.medengphy.2008.09.004

42. Oungoulian SR, Durney KM, Jones BK, Ahmad CS, Hung CT, Ateshian GA. Wear and damage of articular cartilage with friction against orthopedic implant materials. *J Biomech*. 2015;48(10):1957-1964. doi:10.1016/j.jbiomech.2015.04.008

43. Fornalski S, Lee TQ. Anatomy and Biomechanics of the Elbow Joint. 2003;7(4):168-178.

44. Kvist J, Thomeé R. *Structured Rehabilitation Model with Clinical Outcomes After ACL Reconstruction*.; 2014. doi:10.1007/978-3-642-36801-1

45. Batlle JA, Cerezal L, Dolores M, et al. The elbow : review of anatomy and common collateral ligament complex pathology using MRI. 2019;7.

46. Contact Stress Analysis of the Elbow Joint ; Design of Radial Head Replacements. *Clin Orthop*. 2011;(567):2011-2011.

47. Langohr GDG, Willing R, Medley JB, King GJW, Johnson JA. The Effect of Radial Head Hemiarthroplasty Geometry on Proximal Radioulnar Joint Contact Mechanics. *J Hand Surg Am*. 2016;41(7):745-752. doi:10.1016/j.jhsa.2016.05.001

48. Shannon HL. The Contact Mechanics and Kinematics of Radial Head Implants. 2012;Master of(Paper 745):60-66. http://ir.lib.uwo.ca/etd/745.

49. Irish SE, Langohr GDG, Willing R, King GJ, Johnson JA. Implications of radial head hemiarthroplasty dish depth on radiocapitellar contact mechanics. *J Hand Surg Am*. 2015;40(4):723-729. doi:10.1016/j.jhsa.2015.01.030

50. Langohr GDG, Willing R, Medley JB, Johnson JA, King GJW. The Effect of Radial Head

Hemiarthroplasty Geometry on Radiocapitellar Joint Contact Mechanics. *J Shoulder Elb Surg*. 2015;24(4):e118. doi:10.1016/j.jse.2014.11.024

51. van Grunsven W, Hernandez-Nava E, Reilly G, Goodall R. Fabrication and Mechanical Characterisation of Titanium Lattices with Graded Porosity. *Metals (Basel)*. 2014;4(3):401-409. doi:10.3390/met4030401

52. De LMR. Evaluation of bone ingrowth into porous titanium implant : histomorphometric analysis in rabbits. 2010;24(4):399-405.

53. Rahimizadeh A, Nourmohammadi Z, Arabnejad S, Tanzer M, Pasini D. Porous architected biomaterial for a tibial-knee implant with minimum bone resorption and bone-implant interface micromotion. *J Mech Behav Biomed Mater*. 2018;78(November 2017):465-479. doi:10.1016/j.jmbbm.2017.11.041

54. Yan C, Hao L, Hussein A, Raymont D. Evaluations of cellular lattice structures manufactured using selective laser melting. *Int J Mach Tools Manuf*. 2012;62:32-38. doi:10.1016/j.ijmachtools.2012.06.002

55. Pan C, Han Y, Lu J. Design and optimization of lattice structures: A review. *Appl Sci*. 2020;10(18):1-36. doi:10.3390/APP10186374

56. Obadimu SO, Kourousis KI. Compressive behaviour of additively manufactured lattice structures: A review. *Aerospace*. 2021;8(8). doi:10.3390/aerospace8080207

57. Abd Malek NMS, Mohamed SR, Che Ghani SA, Wan Harun WS. Critical evaluation on structural stiffness of porous cellular structure of cobalt chromium alloy. *IOP Conf Ser Mater Sci Eng*. 2015;100(1). doi:10.1088/1757-899X/100/1/012019

58. Hazlehurst K, Wang CJ, Stanford M. Evaluation of the stiffness characteristics of square pore CoCrMo cellular structures manufactured using laser melting technology for potential orthopaedic applications. *Mater Des*. 2013;51:949-955. doi:10.1016/j.matdes.2013.05.009

59. Wang L, Kang J, Sun C, Li D, Cao Y, Jin Z. Mapping porous microstructures to yield desired mechanical properties for application in 3D printed bone scaffolds and orthopaedic implants. *Mater Des*. 2017;133:62-68. doi:10.1016/j.matdes.2017.07.021

60. Choren JA, Heinrich SM, Silver-Thorn MB. Young's modulus and volume porosity relationships for additive manufacturing applications. *J Mater Sci*. 2013;48(15):5103-5112. doi:10.1007/s10853-013-7237-5

61. Tapscott DC, Wottowa C. Orthopedic Implant Materials. *StatPearls*. July 2021. https://www.ncbi.nlm.nih.gov/books/NBK560505/. Accessed November 24, 2021.

62. Mehboob H, Tarlochan F, Mehboob A, Chang SH. Finite element modelling and characterization of 3D cellular microstructures for the design of a cementless biomimetic porous hip stem. *Mater Des*. 2018;149:101-112. doi:10.1016/j.matdes.2018.04.002

63. Luxner MH. Numerical simulations of 3D open cell structures – influence of structural irregularities on elasto-plasticity and deformation localization. 2007;44:2990-3003. doi:10.1016/j.ijsolstr.2006.08.039

64. Parthasarathy J, Starly B, Raman S, Christensen A. Mechanical evaluation of porous titanium (Ti6Al4V) structures with electron beam melting (EBM). *J Mech Behav Biomed Mater*. 2010;3(3):249-259. doi:10.1016/j.jmbbm.2009.10.006

65. Limmahakhun S, Oloyede A, Sitthiseripratip K, Xiao Y, Yan C. 3D-printed cellular structures for bone biomimetic implants. *Addit Manuf*. 2017;15:93-101. doi:10.1016/j.addma.2017.03.010

66. Yan C, Hao L, Hussein A, Bubb SL, Young P, Raymont D. Evaluation of light-weight AlSi10Mg periodic cellular lattice structures fabricated via direct metal laser sintering. *J Mater Process Technol*. 2014;214(4):856-864. doi:10.1016/j.jmatprotec.2013.12.004

67. Wendy Gu X, Greer JR. Ultra-strong architected Cu meso-lattices. *Extrem Mech Lett*. 2015;2(1):7-14. doi:10.1016/j.eml.2015.01.006

68. Tao W, Leu MC. Design of lattice structure for additive manufacturing. *Int Symp Flex Autom ISFA 2016*. 2016;(November 2018):325-332. doi:10.1109/ISFA.2016.7790182

69. Tancogne-Dejean T, Spierings AB, Mohr D. Additively-manufactured metallic micro-lattice materials for high specific energy absorption under static and dynamic loading. *Acta Mater*. 2016;116:14-28. doi:10.1016/j.actamat.2016.05.054

70. Hailu YM, Nazir A, Lin SC, Jeng JY. The effect of functional gradient material distribution and patterning on torsional properties of lattice structures manufactured using multijet fusion technology. *Materials (Basel)*. 2021;14(21):1-21. doi:10.3390/ma14216521

71. Soltani-Tehrani A, Lee S, Sereshk MRV, Shamsaei N. Effects of unit cell size on the mechanical performance of additive manufactured lattice structures. *Solid Free Fabr 2019 Proc 30th Annu Int Solid Free Fabr Symp - An Addit Manuf Conf SFF 2019*. 2019:2254-2262.

72. Jetté B, Brailovski V, Dumas M, Simoneau C, Terriault P. Femoral stem incorporating a diamond cubic lattice structure: Design, manufacture and testing. *J Mech Behav Biomed Mater*. 2018;77(August 2017):58-72. doi:10.1016/j.jmbbm.2017.08.034

73. Heinl P, Müller L, Körner C, Singer RF, Müller FA. Cellular Ti-6Al-4V structures with interconnected macro porosity for bone implants fabricated by selective electron beam melting. *Acta Biomater*. 2008;4(5):1536-1544. doi:10.1016/j.actbio.2008.03.013

74. Hazlehurst KB, Wang CJ, Stanford M. A numerical investigation into the influence of the properties of cobalt chrome cellular structures on the load transfer to the periprosthetic femur following total hip arthroplasty. *Med Eng Phys*. 2014;36(4):458-466. doi:10.1016/j.medengphy.2014.02.008

75. Kodir K, Tanti I, Odang RW, Shulpekov AM, Kashapov LN, Kashapov NF. Critical evaluation on structural stiffness of porous cellular structure of cobalt chromium alloy Critical evaluation on structural stiffness of porous cellular structure of cobalt chromium alloy. 2015. doi:10.1088/1757-899X/100/1/012019

76. Gibson LJ, Editor G. C ellular Solids. 2021;(APRIL 2003):270-274.

77. Fuglsang Nielsen L. Elasticity and damping of porous materials and impregnated materials. *J Am Ceram Soc*. 1983;67:93-98.

78. Head R. EVOLVE Proline Plus Radial Head and Repair System.

79. Pereira TF, Oliveira MF, Maia IA, Silva JVL, Costa MF, Thiré RMSM. 3D printing of poly(3-hydroxybutyrate) porous structures using selective laser sintering. *Macromol Symp*. 2012;319(1):64-73. doi:10.1002/masy.201100237

80. Savalani MM, Hao L, Zhang Y, Tanner KE, Harris RA. Fabrication of porous bioactive structures using the selective laser sintering technique. *Proc Inst Mech Eng Part H J Eng Med*. 2007;221(8):873-886. doi:10.1243/09544119JEIM232

81. Mazzoli A. Selective laser sintering in biomedical engineering. *Med Biol Eng Comput*. 2013;51(3):245-256. doi:10.1007/s11517-012-1001-x

82. Chin HC, Khayat G, Quinn TM. Improved characterization of cartilage mechanical properties using a combination of stress relaxation and creep. *J Biomech*. 2011;44(1):198-201. doi:10.1016/j.jbiomech.2010.09.006

83. Lanting BA, Ferreira LM, Johnson JA, King GJ, Athwal GS. Clinical Biomechanics Radial head implant diameter : A biomechanical assessment of the forgotten dimension. *JCLB*. 2015;30(5):444-447. doi:10.1016/j.clinbiomech.2015.03.012

84. Jansson KS, Michalski MP, Smith SD, LaPrade RF, Wijdicks CA. Tekscan pressure sensor output changes in the presence of liquid exposure. *J Biomech*. 2013;46(3):612-614. doi:10.1016/j.jbiomech.2012.09.033

85. Tancogne-Dejean T, Mohr D. Stiffness and specific energy absorption of additively-manufactured metallic BCC metamaterials composed of tapered beams. *Int J Mech Sci*. 2018;141(February):101-116. doi:10.1016/j.ijmecsci.2018.03.027

86. Zhao M, Liu F, Fu G, Zhang DZ, Zhang T, Zhou H. Improved mechanical properties and energy absorption of BCC lattice structures with triply periodic minimal surfaces fabricated by SLM. *Materials (Basel)*. 2018;11(12). doi:10.3390/ma11122411

87. Thibault M, Poole AR, Buschmann MD. Cyclic compression of cartilage / bone explants

in vitro leads to physical weakening , mechanical breakdown of collagen and release of matrix fragments. 2002;20:1265-1273.

Chapter 2

2 Design and Development of a Radial Head Hemiarthroplasty Implant with a Porous Internal Lattice Structure and Thin Outer Shell

This chapter presents the design and development of a low stiffness hemiarthroplasty implant with an internal lattice structure and thin outer shell. Included is a brief summary of the relevant parameters of a lattice structure and the associated contributions to a porous structures' mechanical properties. The design characteristics of the proposed hemiarthroplasty implant used for assessment are then discussed followed by the subsequent evaluation of their mechanical properties. This chapter also outlines the fabrication techniques used to construct the porous radial head hemiarthroplasty implants which will be used to conduct the study presented in Chapter 3 of this dissertation.

2.1 Introduction

High stiffness metal implants are thought to be an important cause of accelerated cartilage wear on the opposing articular surface[8,37–39]. The use of porosity via structural lattice design has been of great interest in recent years to improve orthopedic implant compliance by mimicking the mechanical properties of bone. Porous surfaces have also been commonly employed for bony ingrowth fixation. Recent investigations have been conducted with a focus on the efficacy of using porosity to prevent complications such as stress shielding, bone resorption, and implant loosening as well as to promote implant osseointegration[31,33,53]. Research however has yet to be conducted on the stiffness reduction of hemiarthroplasty implants using porosity via structural lattice designs to prevent the acceleration of articular cartilage.

As discussed in **Chapter 1**, studies have indicated that a significant reduction in implant stiffness, below a threshold of ~0.3GPa is needed to reduce contact stresses at the implant – cartilage interface and to ultimately preserve articular cartilage health. Recent studies on the evaluation of mechanical properties of porous structures have revealed that implementation of a porous lattice structure is an effective tool in generating effective stiffness values markedly lower than the solid

form[57–59,62–64,65]. Wang et al., reported a stiffness reduction of approximately 75 – 80% via compressive testing of square porous Ti6Al4V structures[59]. Parthasarathy et al., reported similar findings in which 50 – 70% porous Ti6Al4V structures generated compressive stiffness values within the range of cortical and trabecular bone and suggests that even minor changes in the lattice structure can decrease stiffness by approximately 80%[64]. Malek et al., conducted a study on the critical evaluation of structural stiffness of porous structures using Cobalt-Chrome-Molybdenum (CoCrMo) revealing a marked reduction in the Young's modulus and Hazlehurst et al., performed a similar study suggesting that porous CoCrMo structures can generate similar stiffness values to femoral cortical and trabecular bone[57,58].

Lattice structures have several advantageous mechanical properties making them suitable for a number of applications, namely medical products[54–56,66]. Lattice structures have impressive stiffness and strength despite having a relatively lightweight structure. In comparison to a solid structure, a lattice structure typically has significantly lower stiffness and strength however these mechanical properties can be optimized through design parameters such as the employed unit cell shape, size, and thus volume fraction of porosity enabling porous structures to satisfy various application requirements[54,59,62,66]. In some cases, as in a study performed by Gu et al., a lattice structure can generate a higher compressive yield strength than the bulk material[67]. Lattice structures also display high energy absorption properties due to the lattices ability to undergo deformation in response to stress. The energy absorption capabilities vary depending on the type of lattice and subsequent components, though research suggests exceptional energy absorption characteristics under static and dynamic loading for various lattice designs[55,68,69].

In light of the forgoing, employing a structural lattice design can effectively reduce the stiffness of solid structure and may be able to optimize articular biomechanics and prevent accelerated

cartilage wear in hemiarthroplasty implants. The design of a lattice structure is integral in developing hemiarthroplasty implants with low stiffness to match with the surrounding bone while having sufficient strength to endure the physiologic loads of daily activities. Important lattice design characteristics include unit cell geometry, and topology, which have considerable affects on the resulting mechanical properties. Understanding the different mechanisms affecting a lattice structures' mechanical properties is vital in gaining insight on the expected biomechanical behaviours of a porous implant. While implant strength is not the principal focus of this thesis, the strength characteristics of the porous lattice structure were considered to avoid potential failure modes during experimental testing.

This chapter discusses the design and development of the internal lattice structure implemented in hemiarthroplasty implants of the radial head as described in **Chapter 1**. In doing so, the different types of lattice structures, their components, and relevant findings on their associated biomechanical performance, as well as the evaluation of a lattice structures effective modulus are also discussed concurrently with the design of the proposed hemiarthroplasty implant. This approach is novel in its application and there are no current studies indicating the effect of porosity on articular biomechanics such as cartilaginous stresses and wear.

2.2 Lattice Structures

Lattice structures are porous bodies or materials formed through the repeated arrangement of unit cells in a given design space[55,56]. The properties of a lattice structure are directly related to the unit cell shape, size, structure, and spatial arrangement. There are a wide range of different unit cell types that can be used to create a lattice structure. Some of the most common unit cells include the body-centered cubic (BCC), face-centered cubic (FCC), simple cubic, and Kelvin (KV) unit cell. These unit cells as well as their resulting lattice structures are shown in Figure 2.1[56].

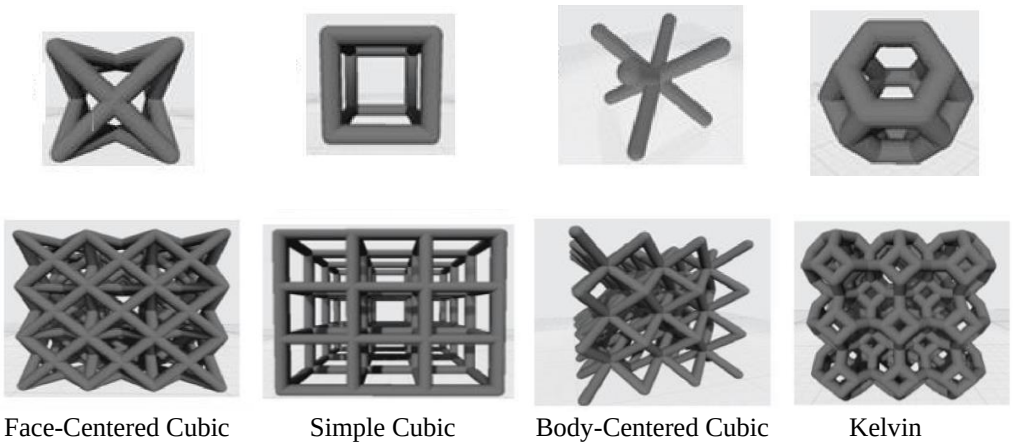

Figure 2.1 – Commonly Used Unit Cell Structures and Resulting lattice Structures
The unit cells and lattice structures shown are the (a) FCC (b) Simple Cubic (c) BCC and (d) KV structures.

A lattice structure can be classified based on the geometry of the repeating unit cell as well as the order by which the unit cells make up the lattice frame. These classifications include[55,56,68].

(1) Periodic Lattices - all unit cells in the lattice are the same shape, size, and topology and are arranged periodically within the lattice structure.

(2) Pseudo-Periodic Lattices - unit cells in the lattice are different shapes and sizes but share the same topology and are arranged periodically within the lattice structure.

(3) Randomized Lattices - unit cells in the lattice are different sizes, and topologies and are randomly distributed throughout the lattice structure.

Lattice structures can be further classified as uniform or non-uniform referring to the unit cell distribution in the lattice. A uniform lattice structure contains uniformly distributed unit cells with the same topological shape and size. In a non-uniform lattice structure, unit cells are unevenly distributed in space and have different topological shapes and geometric sizes as shown in Figure 2.2[55].

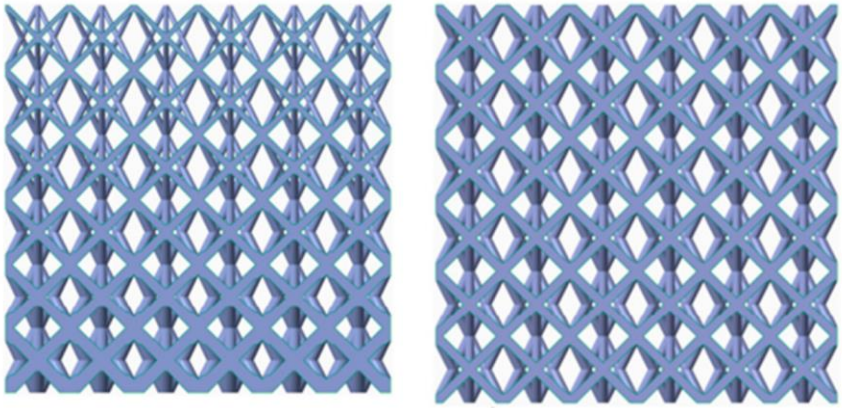

(a) (b)

Figure 2.2 - Non-Uniform (a) and Uniform (b) Lattice Structure[55]

Finally, lattice structures can be built using direct patterning, conformal patterning, or topology optimization[68,70].

(1) Direct Patterning – unit cells are repeated translationally.

(2) Conformal Patterning – unit cells are repeated such that they conform to a given design space.

(3) Topology Optimization – a method that allows of the optimization of the material distribution of a single unit cell and the spatial replication of unit cells within a design space.

Direct patterning is commonly used when filling a simple design volume such that the lattice is encased in a solid material. A conformal lattice, however, is used to create a porous structure in the shape of a given design volume. Conformal lattices allow for the preservation of unit cell integrity as well as the stiffness and strength properties of a porous structure[68].

2.3 Structural Lattice Design for a Porous Radial Head Implant

A uniform lattice structure was used to create the internal lattice structure for a porous radial head hemiarthroplasty presented in this thesis. Direct patterning was used as the method of implementing the lattice into the underlying implant structure such that the outer shell of the implant remains solid. A uniform lattice structure was used due to the simplicity in the design and manufacturing process, and the ability to translate findings to more complex lattice designs and has also been shown to produce relatively uniform mechanical properties while subject to uniaxial compressive load. Furthermore, a uniform lattice structure contains uniform unit-cell strut orientations limiting the variability in the biomechanical behaviour of the lattice under a given loading condition and allowing for analysis of these behaviours at the unit cell level[27].

2.3.1 Unit Cell Shape

Each type of unit cell has a unique set of characteristics that affect the mechanical performance of a lattice structure. The unit cell alone plays an integral role in the mechanical properties and structural characteristics of a lattice[55,56]. There are a substantial number of unit-cell structures that currently exist however, research has been mostly on the optimization of unit cell design and arrangement such that it is able to satisfy a specific set of requirements. Limited research has been conducted on the comparative mechanical performances of different lattice structures[56].

A BCC unit cell was used to create the internal lattice structure for a radial head implant design employed in this thesis. BCC unit cells are one of the most highly recognized unit cells in lattice design and provide a good representation of the expected biomechanical performance of a lattice structure which can be translated to other lattice designs alike. To confirm their distinctiveness, Obadimu et al., conducted a comprehensive review on over 70 studies that investigate the compressive behaviour of lattice structures. Their findings reported that the BCC lattice was the

most commonly used model identified in the literature[56,71]. Mehboob et al. conducted a finite element study in which three different unit cell structures, BCC, Cubic and Diamond, were tested to determine which would yield the best mechanical performance in the context of a hip stem[62]. Compared to the cubic and diamond unit cell structures, the BCC unit cell demonstrated enhanced and moderately isotropic mechanical properties with respect to compressive, bending, and torsional stiffness[59,62,63]. The isotropic nature of a BCC unit cell reduces the variability in mechanical behaviour when subject to a range of loading conditions as in hemiarthroplasty implants[59]. The BCC unit cell was reported to also be able to generate an optimal mechanical performance closest to that of the native state. The BCC unit cell has been further compared to other unit cell structures such as the KV, Reinforced Body Centered Cubic (RBCC), Gibson Ashby (GA), and Weaire Phelan (WP) unit cells. The BCC unit cell was found to provide enhanced controllability of porosity relative to the other designs[63]. In other studies, the BCC unit cell has yielded poor mechanical performance. That said, researchers have developed several optimization techniques introducing enhanced lattice models with improved structural characteristics largely based on the BCC model[56]. In the future, this hemiarthroplasty design could therefore be modified to a multitude of other lattice types to further determine their affect on articular biomechanics.

2.3.2 Unit Cell Size

The unit cell size has an important influence on both the mechanical properties of the lattice structure and the manufacturability. With respect to the mechanical performance of a lattice, the phenomenon that “smaller is stronger” is commonly employed, such that a smaller unit cell size increases the density, stiffness, and strength of the structure[54,62,66]. Unit cell size becomes an important consideration in matching the stiffness of the porous structure to that of natural bone[71]. The size of the unit cell also dictates the number of unit cells present in the lattice. Increasing the

number of unit cells in the lattice with a constant volume has been shown to increase the lattices' energy absorption capabilities and cause less deformation under similar compressive loading conditions[71].

The porous radial head implants used in this thesis were constructed using a 4 x 4 x 4 mm unit cell. This was chosen to maximise the number of unit cells in the lattice whilst considering the manufacturability of the lattice and the resulting stiffness and strength characteristics. A 4 mm^3 unit cell size has become an experimental standard used by many in the evaluation of porous structures as it is able to adequately represent the behaviour of a infinite structure[54,62,63,66]. Soltani-Tehrani et al., reported successful manufacturing of a BCC lattice with unit cells 4 mm^3 in size using the laser beam powder bed fusion technology (LB-PBF)[71]. Yan et al., also reported that unit cells within the range of 2 – 8 mm can be adequately manufactured free of any defects by the selective laser melting (SLM) process[54].

2.3.3 Porosity Variations

To modify the porosity of the implants designed and assessed in this thesis, the unit cell size was kept constant. Only the internal strut diameter of the BCC unit cell was modified such that increasing strut size decreased the volume fraction of porosity in the implant structure. An alternative method of creating porosity variations within a lattice structure uses a constant volume fraction with variable unit cell size and strut size. This method introduces challenges in the manufacturability of the lattice structure. To maintain a constant volume fraction, porosity variations are implemented by decreasing unit cell size which requires a decrease in internal strut diameter thus increasing the likelihood of finding broken cells in the lattice[66].

A 0.4 mm, 0.6 mm, and 0.9 mm internal strut diameter was used to vary the porous volume fraction of the BCC lattice as done by Wang et al., and Mehboob et al., and will be referred to as BCC4, BCC6, and BCC9 herein[59,62]. The outlined strut dimensions represent porosities of 80, 74, and 65%, respectively. The US Food and Drug Administration (FDA) approved a minimum and maximum porosity range of 40 – 70% for femoral components designed for increased biological fixation. This range was used to approximate an appropriate porosity range for the presented thesis[72]. This range however does not encapsulate extreme high and low material properties of bone as in athletes or osteoporotic patients in which that maximum allowed porosity may be extended up to 90% for enduring physiologic loading conditions and experiencing similar biomechanical behaviour to bone[62]. Manufacturability was also taken into consideration in determining an appropriate range of porosities for this thesis. Processing limits for L-PBF and other manufacturing techniques alike have suggested that ordered porous structures in the medium to high range (i.e., 40 – 80%) would yield in the highest manufacturing reliability. Porosities below this range would likely lead to enclosed pores within the structure due to complications in removing excess powder during or after the build[29]. Finally, native bone tissue consists of a solid cortical shell with a trabecular core. Trabecular bone is a porous tissue with interconnected porosity between 55-70%[73]. While the goal of this thesis was not to model bone, it was thought that employing a similar porosity range would increase the likelihood of generating contact mechanics like the native state.

2.4 Evaluation of Relevant Porous Mechanical Properties

The Young's modulus is of particular interest as per previous findings that suggest a reduction in implant stiffness can improve hemiarthroplasty implant compliance[57,58,74]. A single equation yielding reliable and consistent results with respect to a specific lattice design does not yet exist. Thus, the effective Young's moduli of the proposed radial head implants were approximated using two methods which have been commonly used in research involving the relationship between porosity and stiffness. Both methods have gained significant recognition in research yielding similar results to those generated in computational and experimental studies[29,54,58,59,62,75].

The Gibson and Ashby model is a simpler quantification of the effective stiffness of the porous structure based on the volume fraction of porosity alone[76]. This model was also developed to predict the elastic moduli of cellular structures with porosities of 70% and above which fit well with the porosity ranges used herein. As shown in Eq. (2.1), this model describes the effective modulus of a porous structure as a relationship between the modulus of the solid material and the square of the porous volume fraction.

$$E_{eff} = E_s(1 - \varphi)^2 \qquad \text{Eq. (2.1)}$$

The Neilson Equation incorporates geometric considerations which can greatly influence the biomechanical behaviour of the porous structure[77]. As in Eq. (2.2), the effective modulus of a porous structure is expressed as the relationship between the modulus of the solid material (E_s), the volume fraction of porosity (φ) and the shape factor of the pores (f).

$$E_{eff} = E_s * \frac{(1-\varphi)^2}{\left(1+\frac{\varphi}{f-1}\right)}; \quad \varphi = \frac{V_p}{V_s+V_p} \qquad \text{Eq. (2.2)}$$

The shape factor describes how efficiently the solid phase of a material can transfer load without considerable amounts of stress concentrations and can have a value between 0 and 1[77]. As shown in Table 2-1, a shape factor of 0 is an extreme case where pores surround solid particles and is therefore extremely inefficient in transferring load. When the shape factor approaches values closer to 1 the material gains a higher level of structural integrity and becomes increasingly reliable in its ability to withstand applied stress.

Table 2-1 - Orders of Magnitude of Shape Factor for Porous Materials as a Function of Pore Geometry [77]

Predominant geometry of pores at small volume fractions	*Shape factor, ρ*	*Comments*
Enveloping network tending to sub-divide solid phase into particles	Low (0 – 0.4)	Shell-like pore networks and compart solid particles decrease the magnitude of ρ
Dendrites / Ribbons	Medium (0.3 – 0.7)	Coarser and more compact pore geometry increases the magnitude of ρ
"Pockets" defined by an enveloping network of the solid phase	High (0.6 – 1.0)	Shell-like solid networks and pore "pockets" of compact shapes increase the magnitude of ρ

2.4.1 The Effective Modulus of Porous Radial Head Implants

The effective moduli of the porous radial head implants were calculated using the Gibson and Ashby model as well as the Nielsen Equation. The calculated stiffness values by both equations are presented in Figure 2.3. A constant value for shape factor of 0.6 was used as the pore shape remained constant getting slightly smaller as the internal strut diameter increased. Each porous structure falls within the medium-high range – as indicated in Table 1 – where the porous phase of the implant is dominant to the solid phase while still able to effectively transfer load.

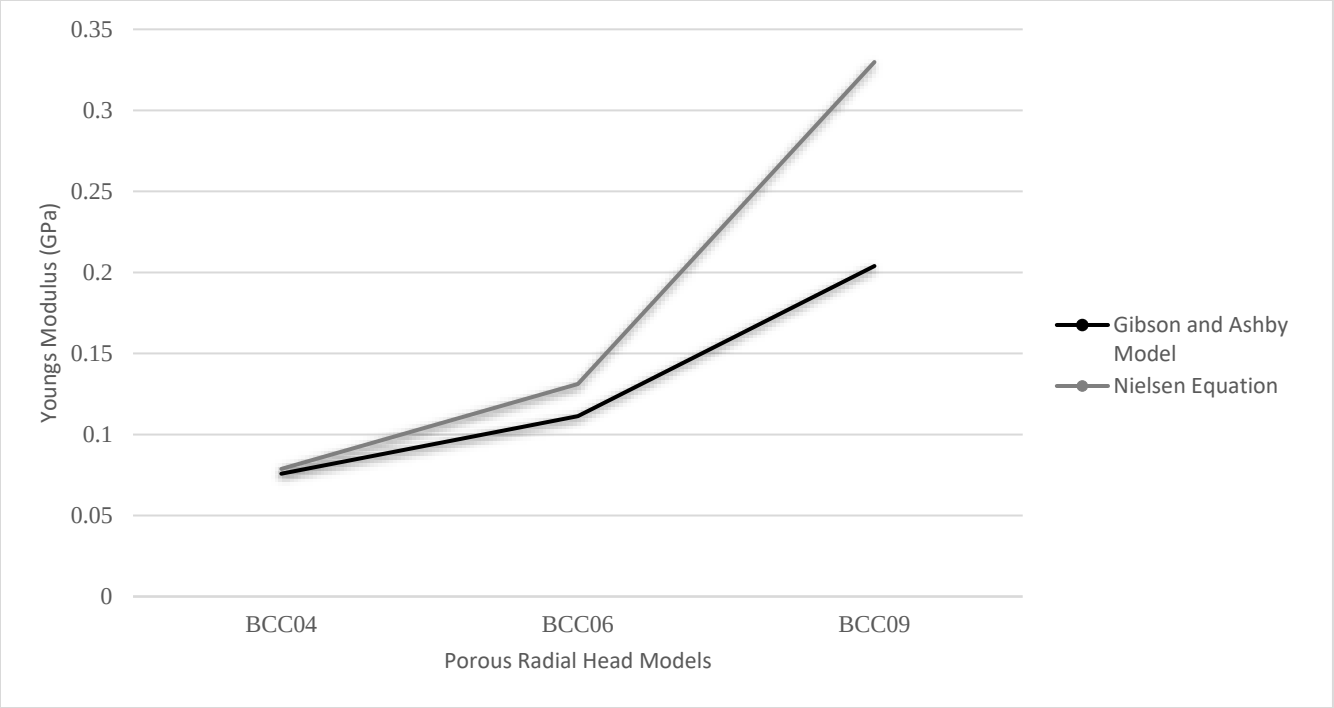

Figure 2.3 - The Relationship Between Porosity and Young's Modulus of Porous Radial Head Implants

The effective modulus of each porous radial head model was calculated using the Gibson and Ashby Model as well as the Nielsen Equation employing a constant shape factor of 0.6.

Both the Nielsen Equation and the Gibson and Ashby Model suggest an 80-90% decrease in effective stiffness of the porous models compared to the solid model. It is expected that the percent decrease found using the Nielsen Equation and the Gibson and Ashby model would be slightly lower as for the solid outer shell. That said, this finding is aligned with the 75 – 80% decrease in stiffness reported by Mehboob et al., using a BCC structure with similar porosity ranges and internal strut diameters. Exact stiffness values generated by similar studies can not be compared as different design geometries and materials were used.

2.5 Implant Design

The Evolve^{TM} Proline Radial Head System (Wright Medical), shown in Figure 2.4, was used as the underlying implant structure in which a uniform BCC internal lattice structure was implemented. The radial head implant was first modeled in Solidworks (SW) (2021, Dassault Systèmes, US) and imported into nTopology (2020, EULA, Version 3.16.2) an engineering design software used for advanced additive manufacturing.

***Figure 2.4 - The Evolve Proline Radial Head System* (Wright Medical, 2007)**
The 24 mm radial head implant size was used to construct the porous hemiarthroplasty implant with a thin articular surface.

The BCC lattice was implemented into each radial head implant with a 0.5 mm outer shell. A fully porous hemiarthroplasty structures would likely increase friction at the implant – cartilage interface, causing stress concentrations to occur at pore sites, and produce larger volumes of articular cartilage wear[31]. A thin articular shell also facilitates uniform distribution of the load through the struts of the lattice[71]. A study conducted by Johnson et al., suggests that a 0.25 mm shell thickness can generate optimal implant compliance and considerably lower hemiarthroplasty contact stresses[31]. Additional findings reported by Berkmortel et al., suggest no significant difference in articular contact mechanics when the shell thickness was 0.25 and 0.5 mm[7]. Thus, a

0.5 mm shell thickness was used to avoid possible implant failure due to insufficient strength without interfering with the biomechanical behaviour of the lattice while under compressive load.

As previously discussed, a 4 mm^3 BCC unit cell was used as the single repeatable unit to create the internal lattice structure for a porous radial head implant presented in this thesis. Shown in Figure 2.5, the internal struts of the BCC lattice contained a circular cross-section which were modified to diameter sizes 0.4 mm, 0.6 mm and 0.9 mm with porosities of 80%, 74%, and 65% respectively.

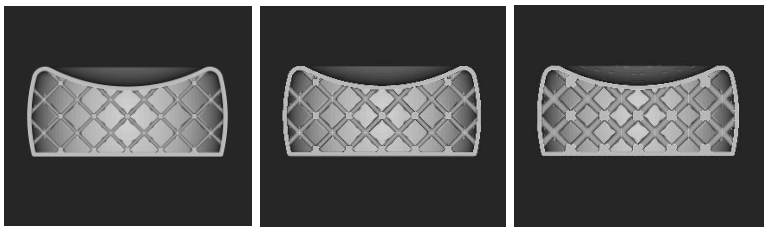

BCC4 *BCC6* *BCC9*

Figure 2.5 – Hemiarthroplasty Implants of the Radial Head with a BCC Internal Lattice Structure and Thin Outer Shell

The BCC4, BCC6, and BCC9 models shown, correspond to 0.4mm, 0.6mm, and 0.9mm internal strut diameter sizes and 80%, 74%, and 65% respectively. The thickness of the outer shell was 0.5mm.

2.6 Implant Fabrication

The three radial head constructs with internal lattice structures were 3D printed along with a solid model of identical geometry using selective laser sintering (SLS) technology. SLS is one of many additive manufacturing technologies which processes polymers, ceramics, metals, and their composites to generate 3-dimensional parts[79,80,81]. The process is performed using a CO_2 laser beam that writes successive layers of a digital model onto a series of deposited powder layers. The laser beam scans the slice geometries onto the powder layers which are then defined by a selective sintering process using a combination of laser and thermal energy. The laser beam penetrates successive layers of powder fusing the powder particles together to form the final part. During the build process, the excess powder provides the 3-dimensional part with structural support to prevent build failures before the sintering process is complete. Once the SLS process is complete, the part is removed from the powder environment and excess powder is removed from the part. Successful fabrication of porous structures via the SLS process have been reported with geometric parameters very close to the digital model and free of delamination (where slices are not fused together)[79,80,81]. The SLS process has also been shown to be an asset in implant design with advanced capabilities in generating complex geometries with a high degree of accuracy and control[81].

In the printing of the porous radial head implants, small circular holes were included on the top and bottom faces of the digital model to allow excess powder to drain out of the part during the build process and prevent unwanted fusion of powder particles. Once the build process was complete, air was blown through the preconstructed holes at a high pressure, to actively remove excess powder that may have adhered to the part walls during the build process. A bright light was also used to visualize the internal lattice structure and highlight areas of high density which would

reveal remaining unwanted powder as well as potential delamination or fractured struts in the lattice.

For this thesis we chose to employ mid-modulus polymeric-based materials to fabricate the implants with the structural modifications described. These implants were then assessed to determine their ability to improve articular contact mechanics (*viz.* contact area and stress) and hence improve compliance. If improvements were found, this would logically lead to the development of future designs using a broad spectrum of implant materials currently employed clinically. For these investigations, the porous models were printed out of polyamide PA2200. PA2200 has a modulus of 1.64 GPa which is consistent with the mid – modulus range of 0.7 GPa – 20.0 GPa for commonly employed polymeric implant materials such as UHMWPE and PyC which are approved for clinical use. Hence, PA2200 was employed as a surrogate material for bench-top testing to mimic these materials. A solid model was also printed from UHMWPE with a modulus of 0.69 GPa. UHMWPE has a slightly lower effective modulus than PA2200 however, as previously reported, only materials with a modulus less than approximately ~0.3GPa would make a significant difference in mechanical performance[3,7,27]. Utilizing a slightly different material for the solid model was intentional as it may provide further insight into the findings of the study presented in this thesis and would allow for comparative analysis to be conducted between similar studies involving UHMWPE. Previous academic work in the Hand and Upper Limb Center has 3D printed the evolve proline radial head model using UHMPWE and was thus used to reduce manufacturing costs and limit material waste.

2.7 Conclusion

This chapter discusses the design rationale and development of a porous radial head hemiarthroplasty implant with an internal lattice structure and a thin outer shell. Lattice structures provide high stiffness and strength as well as impressive energy absorption characteristics making them suitable for orthopedic applications. The individual characteristics of a lattice structure such as unit cell shape, size, and volume fraction of porosity have significant implications on the resulting mechanical properties and expected biomechanical behaviour. Based on extensive research, a BCC unit cell, 4 mm^3 in size, was used to construct a uniform lattice within the geometric constraints of the Evolve Proline Radial Head System (Wright Medical) with a 0.5 mm uniform shell thickness. Three porous radial head implants were developed by modifying the internal strut diameter of the lattice. Strut sizes of 0.4 mm, 0.6 mm, and 0.9 mm were used corresponding to porosities of 80, 74, and 65% porosity, respectively. SLS technology was used to additively manufacture the porous models using PA2200 (E = 1.64 GPa) and a solid model using UHMWPE (E = 0.69 GPa). The Gibson and Ashby Model and the Nielsen Equation were used to approximate the effective stiffness of the porous radial head hemiarthroplasty implants suggesting an 80 – 90% decrease approximately compared to the solid model. **Chapter 3** presents an in-vivo investigation evaluating the articular biomechanics of the porous radial head implants designed and fabricated as described above.

2.8 References

1. Lavrenko PN, Raglis V V. *Automatic Cassette Diffusometer*. Vol 29.; 1986.

2. Pt TLU, Therapy P, Second S. Hemiarthroplasty Total Shoulder Arthroplasty Imaging of Total Joint Replacement. 2018.

3. Dedecker S. The Efficacy of Bionate as an Articulating Surface for Joint Hemiarthroplasty. 2017;(January):1-85.

4. Bleß HH, Kip M. White paper on joint replacement: Status of hip and knee arthroplasty care in Germany. *White Pap Jt Replace Status Hip Knee Arthroplast Care Ger*. 2017:1-135. doi:10.1007/978-3-662-55918-5

5. Arthritis Foundation. Arthritis by the Numbers. *Arthritis Found*. 2019:1-70. https://www.arthritis.org/getmedia/e1256607-fa87-4593-aa8a-8db4f291072a/2019-abtn-final-march-2019.pdf.

6. Pappas N, Bernstein J. Fractures in brief: Radial head fractures. *Clin Orthop Relat Res*. 2010;468(3):914-916. doi:10.1007/s11999-009-1183-1

7. Berkmortel C. Lower Stiffness Orthopaedic Implants for Hemiarthroplasty. 2020:130.

8. Lizhang J, Fisher J, Jin Z, Burton A, Williams S. The effect of contact stress on cartilage friction, deformation and wear. *Proc Inst Mech Eng Part H J Eng Med*. 2011;225(5):461-475. doi:10.1177/2041303310392626

9. Einhorn TA, Guy- G, Schemitsch EH, et al. new england journal. 2019:2199-2208. doi:10.1056/NEJMoa1906190

10. Robertson GAJ, Wood AM, Wood AM. Hip hemi-arthroplasty for neck of femur fracture : What is the current evidence ? 2018;9(11):235-244. doi:10.5312/wjo.v9.i11.235

11. Jr DJH, Hsu JE, Iii FAM. Primary Shoulder Hemiarthroplasty : What Can Be Learned From 359 Cases That Were Surgically Revised ? 2018:1031-1040. doi:10.1007/s11999.0000000000000167

12. Wagner ER, Farley KX, Higgins I, Wilson JM, Daly CA, Gottschalk MB. The incidence of shoulder arthroplasty : rise and future projections compared with hip and knee arthroplasty. *J Shoulder Elb Surg*. 2020;29(12):2601-2609. doi:10.1016/j.jse.2020.03.049

13. Trofa D, Rajaee SS, Smith EL. Nationwide Trends in Total Shoulder Arthroplasty and Hemiarthroplasty for Osteoarthritis. 2014;(April):166-172.

14. Bekerom MPJ Van Den, Geervliet PC, Somford MP, Den MPJ Van. Original Article Total shoulder arthroplasty versus hemiarthroplasty for glenohumeral arthritis : A systematic review of the literature at long-term follow-up. 2013;7(3):3-8. doi:10.4103/0973-6042.118915

15. Gezeral OS. Prosthesis arthritis toronto,. :244-255.

16. Mccann LÃ, Ingham E, Jin Z, Fisher J. An investigation of the effect of conformity of knee hemiarthroplasty designs on contact stress , friction and degeneration of articular cartilage : A tribological study. 2009;42:1326-1331. doi:10.1016/j.jbiomech.2009.03.028

17. Vance MC, Wolfe SW, Packer G, Tan D, Crisco JJT, Ph D. Midcarpal Hemiarthroplasty for Wrist Arthritis : Rationale and Early Results. 2012;1(212):61-67.

18. Anneberg M, Packer G, Crisco JJ, Wolfe S. Four-Year Outcomes of Midcarpal Hemiarthroplasty for Wrist Arthritis. *J Hand Surg Am*. 2017;42(11):894-903. doi:10.1016/j.jhsa.2017.07.029

19. Jr EGH, Lum Z, Bamberger HB, Trzeciak MA. Failure of Wrist Hemiarthroplasty. 2017. doi:10.1177/1558944716668836

20. Rticle CRA, Beasley J. FOR Osteoarthritis and Rheumatoid Arthritis : Conservative Therapeutic Management. *J Hand Ther*. 2012;25(2):163-172. doi:10.1016/j.jht.2011.11.001

21. Pettersson K, Amilon A, Rizzo M. Pyrolytic Carbon Hemiarthroplasty in the Management of Proximal Interphalangeal Joint Arthritis. *J Hand Surg Am*. 2015;40(3):462-468. doi:10.1016/j.jhsa.2014.12.016

22. Hohman DW, Nodzo SR, Qvick LM, Duquin TR, Paterson PP. Hemiarthroplasty of the distal humerus for acute and chronic complex intra-articular injuries. *J Shoulder Elb Surg*. 2014;23(2):265-272. doi:10.1016/j.jse.2013.05.007

23. Stuffmann E, Baratz ME. Radial Head Implant Arthroplasty. *YJHSU*. 2009;34(4):745-754. doi:10.1016/j.jhsa.2009.01.027

24. Estrada-Malacón CA, Pérez-Valtierra M, Torres-Zavala A, Fonseca-Bernal M. Hemiartroplastía de cúpula radial en pacientes con fractura tipo III y IV según Mason Johnston. *Acta ortopédica Mex*. 2015;29(3):148-154.

25. Kodde IF, Kaas L, Flipsen M, Bekerom MPJ Van Den, Eygendaal D. Current concepts in the management of radial head fractures. 2015;6(11):954-960. doi:10.5312/wjo.v6.i11.954

26. Phadnis J, Watts AC, Bain GI. Elbow hemiarthroplasty for the management of distal humeral fractures: current technique, indications and results. *Shoulder Elb*. 2016;8(3):171-183. doi:10.1177/1758573216640210

27. Khayat A. Effect of Hemiarthroplasty Implant Contact Geometry and Material on Early Cartilage Wear. 2015;(October):1-102.

28. Sahu D, Holmes DM, Fitzsimmons JS, et al. Influence of radial head prosthetic design on radiocapitellar joint contact mechanics. *J Shoulder Elb Surg*. 2014;23(4):456-462. doi:10.1016/j.jse.2013.11.028

29. Dumas M, Terriault P, Brailovski V. Modelling and characterization of a porosity graded lattice structure for additively manufactured biomaterials. *Mater Des*. 2017;121:383-392. doi:10.1016/j.matdes.2017.02.021

30. Disc I, Ligament AC, Tis- B, Bone C, Remodeling B. Learn more about Stress Shielding Responses of Musculoskeletal Tissues to Disuse and Remobilization. 2014.

31. Krishna BV, Bose S, Bandyopadhyay A. Low stiffness porous Ti structures for load-bearing implants. *Acta Biomater*. 2007;3(6):997-1006. doi:10.1016/j.actbio.2007.03.008

32. Matassi F, Botti A, Sirleo L, Carulli C, Innocenti M. Porous metal for orthopedics implants. *Clin Cases Miner Bone Metab*. 2013;10(2):111-115. doi:10.11138/ccmbm/2013.10.2.111

33. Arabnejad S, Johnston B, Tanzer M, Pasini D. Fully porous 3D printed titanium femoral stem to reduce stress-shielding following total hip arthroplasty. *J Orthop Res*. 2017;35(8):1774-1783. doi:10.1002/jor.23445

34. Chanlalit C, Shukla DR, Fitzsimmons JS, An KN, O'Driscoll SW. Stress Shielding Around Radial Head Prostheses. *J Hand Surg Am*. 2012;37(10):2118-2125. doi:10.1016/J.JHSA.2012.06.020

35. Jin H, Lewis JL. Determination of Poisson's Ratio of Articular Cartilage by Indentation Using Different-Sized Indenters. *J Biomech Eng*. 2004;126(2):138-145. doi:10.1115/1.1688772

36. Sophia Fox AJ, Bedi A, Rodeo SA. The basic science of articular cartilage: Structure, composition, and function. *Sports Health*. 2009;1(6):461-468. doi:10.1177/1941738109350438

37. Cruess RL, Kwok DC, Duc PN, Lecavalier MA, Dang GT. The response of articular cartilage to weight-bearing against metal. A study of hemiarthroplasty of the hip in the dog. *J Bone Jt Surg - Ser B*. 1984;66(4):592-597. doi:10.1302/0301-620x.66b4.6204988

38. Chan SMT, Neu CP, Komvopoulos K, Reddi AH, Di Cesare PE. Friction and wear of hemiarthroplasty biomaterials in reciprocating sliding contact with articular cartilage. *J Tribol*. 2011;133(4). doi:10.1115/1.4004760

39. Schwartz CJ, Bahadur S. Investigation of articular cartilage and counterface compliance in multi-directional sliding as in orthopedic implants. 2007;262:1315-1320. doi:10.1016/j.wear.2007.01.007

40. Lawless BM, Sadeghi H, Temple DK, Dhaliwal H, Espino DM, Hukins DWL. Viscoelasticity of articular cartilage: Analysing the effect of induced stress and the restraint of bone in a dynamic environment. *J Mech Behav Biomed Mater*. 2017;75(May):293-301. doi:10.1016/j.jmbbm.2017.07.040

41. Katta J, Jin Z, Ingham E, Fisher J. Biotribology of articular cartilage-A review of the

recent advances. *Med Eng Phys*. 2008;30(10):1349-1363. doi:10.1016/j.medengphy.2008.09.004

42. Oungoulian SR, Durney KM, Jones BK, Ahmad CS, Hung CT, Ateshian GA. Wear and damage of articular cartilage with friction against orthopedic implant materials. *J Biomech*. 2015;48(10):1957-1964. doi:10.1016/j.jbiomech.2015.04.008

43. Fornalski S, Lee TQ. Anatomy and Biomechanics of the Elbow Joint. 2003;7(4):168-178.

44. Kvist J, Thomeé R. *Structured Rehabilitation Model with Clinical Outcomes After ACL Reconstruction*.; 2014. doi:10.1007/978-3-642-36801-1

45. Batlle JA, Cerezal L, Dolores M, et al. The elbow : review of anatomy and common collateral ligament complex pathology using MRI. 2019;7.

46. Contact Stress Analysis of the Elbow Joint ; Design of Radial Head Replacements. *Clin Orthop*. 2011;(567):2011-2011.

47. Langohr GDG, Willing R, Medley JB, King GJW, Johnson JA. The Effect of Radial Head Hemiarthroplasty Geometry on Proximal Radioulnar Joint Contact Mechanics. *J Hand Surg Am*. 2016;41(7):745-752. doi:10.1016/j.jhsa.2016.05.001

48. Shannon HL. The Contact Mechanics and Kinematics of Radial Head Implants. 2012;Master of(Paper 745):60-66. http://ir.lib.uwo.ca/etd/745.

49. Irish SE, Langohr GDG, Willing R, King GJ, Johnson JA. Implications of radial head hemiarthroplasty dish depth on radiocapitellar contact mechanics. *J Hand Surg Am*. 2015;40(4):723-729. doi:10.1016/j.jhsa.2015.01.030

50. Langohr GDG, Willing R, Medley JB, Johnson JA, King GJW. The Effect of Radial Head Hemiarthroplasty Geometry on Radiocapitellar Joint Contact Mechanics. *J Shoulder Elb Surg*. 2015;24(4):e118. doi:10.1016/j.jse.2014.11.024

51. van Grunsven W, Hernandez-Nava E, Reilly G, Goodall R. Fabrication and Mechanical Characterisation of Titanium Lattices with Graded Porosity. *Metals (Basel)*. 2014;4(3):401-409. doi:10.3390/met4030401

52. De LMR. Evaluation of bone ingrowth into porous titanium implant : histomorphometric analysis in rabbits. 2010;24(4):399-405.

53. Rahimizadeh A, Nourmohammadi Z, Arabnejad S, Tanzer M, Pasini D. Porous architected biomaterial for a tibial-knee implant with minimum bone resorption and bone-implant interface micromotion. *J Mech Behav Biomed Mater*. 2018;78(November 2017):465-479. doi:10.1016/j.jmbbm.2017.11.041

54. Yan C, Hao L, Hussein A, Raymont D. Evaluations of cellular lattice structures manufactured using selective laser melting. *Int J Mach Tools Manuf*. 2012;62:32-38. doi:10.1016/j.ijmachtools.2012.06.002

55. Pan C, Han Y, Lu J. Design and optimization of lattice structures: A review. *Appl Sci*. 2020;10(18):1-36. doi:10.3390/APP10186374

56. Obadimu SO, Kourousis KI. Compressive behaviour of additively manufactured lattice structures: A review. *Aerospace*. 2021;8(8). doi:10.3390/aerospace8080207

57. Abd Malek NMS, Mohamed SR, Che Ghani SA, Wan Harun WS. Critical evaluation on structural stiffness of porous cellular structure of cobalt chromium alloy. *IOP Conf Ser Mater Sci Eng*. 2015;100(1). doi:10.1088/1757-899X/100/1/012019

58. Hazlehurst K, Wang CJ, Stanford M. Evaluation of the stiffness characteristics of square pore CoCrMo cellular structures manufactured using laser melting technology for potential orthopaedic applications. *Mater Des*. 2013;51:949-955. doi:10.1016/j.matdes.2013.05.009

59. Wang L, Kang J, Sun C, Li D, Cao Y, Jin Z. Mapping porous microstructures to yield desired mechanical properties for application in 3D printed bone scaffolds and orthopaedic implants. *Mater Des*. 2017;133:62-68. doi:10.1016/j.matdes.2017.07.021

60. Choren JA, Heinrich SM, Silver-Thorn MB. Young's modulus and volume porosity relationships for additive manufacturing applications. *J Mater Sci*. 2013;48(15):5103-5112. doi:10.1007/s10853-013-7237-5

61. Tapscott DC, Wottowa C. Orthopedic Implant Materials. *StatPearls*. July 2021. https://www.ncbi.nlm.nih.gov/books/NBK560505/. Accessed November 24, 2021.

62. Mehboob H, Tarlochan F, Mehboob A, Chang SH. Finite element modelling and characterization of 3D cellular microstructures for the design of a cementless biomimetic porous hip stem. *Mater Des*. 2018;149:101-112. doi:10.1016/j.matdes.2018.04.002

63. Luxner MH. Numerical simulations of 3D open cell structures – influence of structural irregularities on elasto-plasticity and deformation localization. 2007;44:2990-3003. doi:10.1016/j.ijsolstr.2006.08.039

64. Parthasarathy J, Starly B, Raman S, Christensen A. Mechanical evaluation of porous titanium (Ti6Al4V) structures with electron beam melting (EBM). *J Mech Behav Biomed Mater*. 2010;3(3):249-259. doi:10.1016/j.jmbbm.2009.10.006

65. Limmahakhun S, Oloyede A, Sitthiseripratip K, Xiao Y, Yan C. 3D-printed cellular structures for bone biomimetic implants. *Addit Manuf*. 2017;15:93-101. doi:10.1016/j.addma.2017.03.010

66. Yan C, Hao L, Hussein A, Bubb SL, Young P, Raymont D. Evaluation of light-weight AlSi10Mg periodic cellular lattice structures fabricated via direct metal laser sintering. *J Mater Process Technol*. 2014;214(4):856-864. doi:10.1016/j.jmatprotec.2013.12.004

67. Wendy Gu X, Greer JR. Ultra-strong architected Cu meso-lattices. *Extrem Mech Lett*. 2015;2(1):7-14. doi:10.1016/j.eml.2015.01.006

68. Tao W, Leu MC. Design of lattice structure for additive manufacturing. *Int Symp Flex Autom ISFA 2016*. 2016;(November 2018):325-332. doi:10.1109/ISFA.2016.7790182

69. Tancogne-Dejean T, Spierings AB, Mohr D. Additively-manufactured metallic micro-lattice materials for high specific energy absorption under static and dynamic loading. *Acta Mater*. 2016;116:14-28. doi:10.1016/j.actamat.2016.05.054

70. Hailu YM, Nazir A, Lin SC, Jeng JY. The effect of functional gradient material distribution and patterning on torsional properties of lattice structures manufactured using multijet fusion technology. *Materials (Basel)*. 2021;14(21):1-21. doi:10.3390/ma14216521

71. Soltani-Tehrani A, Lee S, Sereshk MRV, Shamsaei N. Effects of unit cell size on the mechanical performance of additive manufactured lattice structures. *Solid Free Fabr 2019 Proc 30th Annu Int Solid Free Fabr Symp - An Addit Manuf Conf SFF 2019*. 2019:2254-2262.

72. Jetté B, Brailovski V, Dumas M, Simoneau C, Terriault P. Femoral stem incorporating a diamond cubic lattice structure: Design, manufacture and testing. *J Mech Behav Biomed Mater*. 2018;77(August 2017):58-72. doi:10.1016/j.jmbbm.2017.08.034

73. Heinl P, Müller L, Körner C, Singer RF, Müller FA. Cellular Ti-6Al-4V structures with interconnected macro porosity for bone implants fabricated by selective electron beam melting. *Acta Biomater*. 2008;4(5):1536-1544. doi:10.1016/j.actbio.2008.03.013

74. Hazlehurst KB, Wang CJ, Stanford M. A numerical investigation into the influence of the properties of cobalt chrome cellular structures on the load transfer to the periprosthetic femur following total hip arthroplasty. *Med Eng Phys*. 2014;36(4):458-466. doi:10.1016/j.medengphy.2014.02.008

75. Kodir K, Tanti I, Odang RW, Shulpekov AM, Kashapov LN, Kashapov NF. Critical evaluation on structural stiffness of porous cellular structure of cobalt chromium alloy Critical evaluation on structural stiffness of porous cellular structure of cobalt chromium alloy. 2015. doi:10.1088/1757-899X/100/1/012019

76. Gibson LJ, Editor G. C ellular Solids. 2021;(APRIL 2003):270-274.

77. Fuglsang Nielsen L. Elasticity and damping of porous materials and impregnated materials. *J Am Ceram Soc*. 1983;67:93-98.

78. Head R. EVOLVE Proline Plus Radial Head and Repair System.

79. Pereira TF, Oliveira MF, Maia IA, Silva JVL, Costa MF, Thiré RMSM. 3D printing of poly(3-hydroxybutyrate) porous structures using selective laser sintering. *Macromol Symp*. 2012;319(1):64-73. doi:10.1002/masy.201100237

80. Savalani MM, Hao L, Zhang Y, Tanner KE, Harris RA. Fabrication of porous bioactive structures using the selective laser sintering technique. *Proc Inst Mech Eng Part H J Eng*

Med. 2007;221(8):873-886. doi:10.1243/09544119JEIM232

81. Mazzoli A. Selective laser sintering in biomedical engineering. *Med Biol Eng Comput*. 2013;51(3):245-256. doi:10.1007/s11517-012-1001-x

82. Chin HC, Khayat G, Quinn TM. Improved characterization of cartilage mechanical properties using a combination of stress relaxation and creep. *J Biomech*. 2011;44(1):198-201. doi:10.1016/j.jbiomech.2010.09.006

83. Lanting BA, Ferreira LM, Johnson JA, King GJ, Athwal GS. Clinical Biomechanics Radial head implant diameter : A biomechanical assessment of the forgotten dimension. *JCLB*. 2015;30(5):444-447. doi:10.1016/j.clinbiomech.2015.03.012

84. Jansson KS, Michalski MP, Smith SD, LaPrade RF, Wijdicks CA. Tekscan pressure sensor output changes in the presence of liquid exposure. *J Biomech*. 2013;46(3):612-614. doi:10.1016/j.jbiomech.2012.09.033

85. Tancogne-Dejean T, Mohr D. Stiffness and specific energy absorption of additively-manufactured metallic BCC metamaterials composed of tapered beams. *Int J Mech Sci*. 2018;141(February):101-116. doi:10.1016/j.ijmecsci.2018.03.027

86. Zhao M, Liu F, Fu G, Zhang DZ, Zhang T, Zhou H. Improved mechanical properties and energy absorption of BCC lattice structures with triply periodic minimal surfaces fabricated by SLM. *Materials (Basel)*. 2018;11(12). doi:10.3390/ma11122411

87. Thibault M, Poole AR, Buschmann MD. Cyclic compression of cartilage / bone explants in vitro leads to physical weakening , mechanical breakdown of collagen and release of matrix fragments. 2002;20:1265-1273.

Chapter 3

3 Effect of a Porous Internal Lattice Design on The Articular Contact Mechanics of Radial Head Hemiarthroplasty Implants

In the previous chapter, the design, development, and fabrication of radial head hemiarthroplasty implants with a structural internal lattice and a thin outer shell was discussed. The methods of evaluation of the effective Young's moduli were also discussed and performed. This chapter presents the mechanical assessment of the articular contact mechanics of radial head implants (against cadaver capitella) with varying porosity as compared to a solid hemiarthroplasty and native radial head. The experimental results consisting of contact area and stress are presented along with a detailed discussion of the associated findings.

3.1 Introduction

As discussed in earlier chapters of this thesis, a significant consequence associated with the use of hemiarthroplasty implants is accelerated cartilage wear at the native articulation. The use of high stiffness metal implants is thought to be the reason for this damage due to the significant mismatch in material properties as compared to the articular cartilage and underlying bone. This mismatch leads to excessive stresses on the opposing cartilage surfaces and may lead to an increasing need for revision surgery due to pain from irreparable cartilage damage and bone. Other potential causes of this accelerated cartilage wear include implant surface roughness and differences in implant geometry relative to the native state[3,27,28,47,49].

Stiffness reduction in orthopaedic implants has become the primary focus for a number of research studies in an effort to maintain articular cartilage health. As in the Hertzian contact stress equation (Eq. 3.1, Eq. 3.2), the contact area is dependent on the moduli of the two materials in contact. As E_2 – the modulus of the implant – decreases, the resultant circular contact area increases. As a result, the maximum contact pressure and maximum principal stress at the center of the articulation decreases as well.

$$a = \frac{\sqrt[3]{3F\left(\frac{1-\gamma_1}{E_1} + \frac{1-\gamma_2}{E_2}\right)}}{4\left(\frac{1}{R_1} + \frac{1}{R_2}\right)} \quad \text{(Eq. 3.1)}$$

Where F is the applied force, γ_1 and γ_2 are the Poisson's ratios, E_1 and E_2 are the young's modulus and R_1 and R_2 are the radii of the two materials in contact.

$$P_{max} = \frac{3F}{2\pi a^2} \quad \text{(Eq. 3.2)}$$

As discussed in **Chapter 1**, Khayat et al., found that materials within the range of 200GPa and 0.69GPa have no significant effect on cartilage wear[27]. Berkmortel et al., reported that materials with stiffness values of ~300 MPa or less would be needed to yield the necessary reduction in cartilage stresses[7]. Furthermore, Dedecker et al., suggested that below 0.69 GPa, implant stiffness likely becomes the predominant factor in producing high volumes of articular cartilage wear[3]. In an attempt to further reduce implant stiffness, Berkmortel et al., employed structural modifications to the radial head hemiarthroplasty however, no significant improvements were found, and the results suggest likely implant failure. Based on the research presented in **Chapter 2,** it is fair to postulate that the structural design of a lattice can provide the necessary reduction in stiffness for notable contact improvements to be made while also providing structural support – via the lattice struts – to prevent the implant from deforming to the point of unwanted stress concentrations or failure.

Introducing porous lattice structures in prosthetic devices has become a promising method in achieving lower stiffness values for orthopedic implants while maintaining sufficient structural strength. The advantageous properties of lattice structure include high stiffness, strength, and energy absorption, as outlined in **Chapter 2**. To add, the parameters of a lattice structure are highly tailorable and can thus be designed to achieve a set of mechanical properties suited to numerous

biomedical and engineering applications. Coupled with the advantageous characteristics provided by a cellular structure, these studies indicate that a porous lattice structure can be used to sufficiently reduce the effective stiffness of an implant, improve articular contact mechanics and reduce cartilage wear[29,57,58]. Implementing a porous internal lattice encased in a thin shell for hemiarthroplasty implants is novel in its application and there are no reported studies to date on the effects of such implants on articular contact mechanics.

Any biomechanical assessment when cartilage is a component of the loaded construct should consider time-related changes in articular load transfer. Cartilage is a viscoelastic material and as such has non-constant articular contact mechanics[40,82]. Studies on native joint contact mechanics are usually evaluated when the applied load becomes stable. This typically occurs after the first few seconds of load application[3,7,27,47–49,83]. Previous studies have investigated the viscoelastic properties of articular cartilage when subjected to compressive loading as well as the wear behaviour of articular cartilage against rigid and compliant materials. Investigations that have examined the time-dependent response at the cartilage-implant interface under compressive load have yet to be conducted. In addition to the potential for changes in contact mechanics to occur over time, it is known that cartilage responds to increasing load in a non-linear fashion approaching a plateau. That said, the appropriate load magnitudes for testing of these constructs have not been fully established.

The purpose of this study was three-fold:

1. To determine the appropriate load magnitude for uniaxial compression testing for radial head hemiarthroplasty implants,
2. To assess the viscoelastic response of the radial head hemiarthroplasty constructs over time,
3. To investigate the effect of implant porosity on articular contact.

As stated in **Chapter 1**, the hypothesis of this study, is that a porous internal lattice structure would reduce the effective stiffness of the implant, thus increasing hemiarthroplasty contact area and reducing contact stress relative to a solid implant

3.2 Methods

The radial head implants developed and described in Chapter 2 were investigated herein. To summarize, this was done by modifying the internal strut diameter of the internal lattice, creating variations in the porosity of each radial head model thereby reducing the effective modulus of the implant. The joint contact mechanics were studied to evaluate if the effective stiffness reduction provided by an internal lattice structure can increase the contact area and reduce the contact stress at the articulation in an effort to prevent rapid cartilage degeneration.

The radii models used in this study were constructed using the 24 mm Evolve Proline Radial Head System (Wright Medical) and additively manufactured using SLS technology (E0S P 396). The mechanical and geometric properties of the radial head hemiarthroplasty implants with a thin 0.5mm outer shell are summarized in Table 3-1. In addition, a solid UHMWPE with an identical external geometry was included to represent a biomaterial that has a modulus in the range of these porous devices.

Table 3-1 – The Geometric Properties of the 3 Porous and the Solid Radial Head Hemiarthroplasty Implants

INTERNAL STRUT DIAMETER (MM)	MATERIAL USED	VOLUME FRACTION OF POROSITY (%)	EFFECTIVE MODULUS (GPA) – *GIBSON AND ASHBY*	EFFECTIVE MODULUS (GPA) – *NEILSEN EQUATION*
0.4	PA2200	80	0.08	0.08
0.6	PA2200	74	0.13	0.11
0.9	PA2200	65	0.33	0.20
SOLID	UHMWPE	0	0.69	0.69

3.2.1 Specimen Preparation, Testing Setup and Procedure

Cadaveric elbow specimens were obtained and dissected to yield denuded radii and capitella (n=11, 69 ± 15, 11M). Each specimen was selected based on CT imaging to confirm radial head sizing and to ensure articular surfaces were free of significant arthritis. The radius and humerus were potted in bone cement in a poly-vinyl chloride tubing and mounted in a custom pneumatic compressive loading apparatus as shown in Figure 3.1. Prior to cementing, the biceps tuberosity of the native radius was marked to ensure proper alignment of the native radial head with respect to the capitellum. Testing was performed at 90-degrees of flexion. A custom Python code was used to apply a uniaxial load using the actuator, compressing the capitellum, against the native, porous, and solid radial head models.

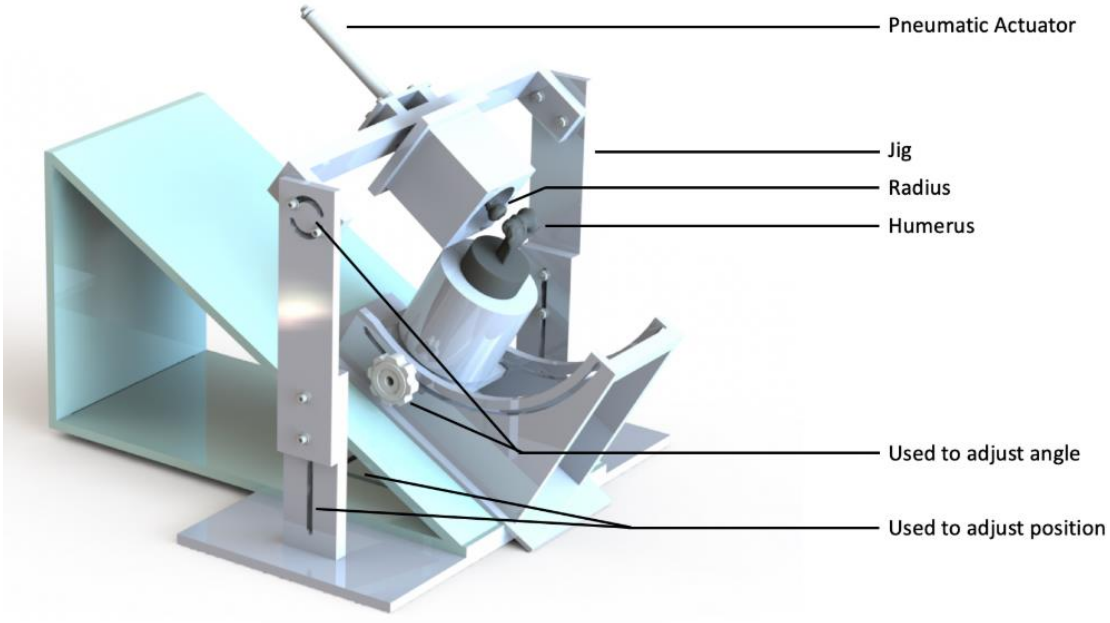

Figure 3.1 - Custom Testing Apparatus
The radial head models and cadaveric humeri were placed in the opposing cylinders at the center of the jig. Using slots on the side of the jig, the position of the radial head models was adjusted for proper articular alignment. The angle was adjusted to 90-degrees using the slots below the humerus.

A Tekscan 5051 sensor (Tekscan, Inc., Boston, MA) was interposed at the articulation and used to quantify the contact area and contact stress (*viz.* pressure) at the joint interface. Prior to testing, the sensor was equilibrated using a bladder membrane that applies a uniform pressure over the entire area of the sensor. This was done to ensure uniform readings across each 1.6129mm^2 square sensel within the sensor. Load calibration was then performed using the pneumatic actuator as per the Tekscan protocol. Calibration was performed at 50N, 100N, 150N and 200N. A series of pilot tests were conducted to ensure repeatability in the outcome measurements. The articulations were kept moist with HyClone® Bovine Calf Serum (ThermoFisher Scientific, Canada) to avoid desiccation during testing. The testing order of the native, solid and porous radial head implants were randomized to avoid the effects of possible cartilage desiccation throughout the testing cycle.

3.2.2 Assessment of Load Magnitude

In order to assess the effect of load magnitude on contact mechanics, a preliminary investigation was conducted. One cadaveric capitellum (n = 1, M, 79yrs.) was articulated against a porous implant model (BCC4, 80% Porosity). The construct was tested via ramp loading at 3 N/s to a maximum of 200N. The Tekscan transducer as discussed in Section 3.2.2 was employed. It was postulated that a non-linear change in both contact area and peak stress would occur, likely due to a combination of creep and stress-relaxation. The purpose of this investigation was to determine an appropriate compressive load to be used for the assessment of the articular contact mechanics of porous constructs as described ahead.

3.2.3 Assessment of The Viscoelastic Response

For this study, eleven human elbow cadaver specimens, as in section 3.2.1, were denuded for harvest of the proximal radius and distal humerus and employed for both this study and the subsequent study (Section 3.2.4). This investigation was performed to assess the contact mechanics

of the native radial head in comparison to those of a solid hemiarthroplasty construct. It was proposed that a non-linear initial response in both the contact stress and area would result followed by an asymptotic settling while under constant applied load. Testing was conducted on all cadaveric specimens for a duration of 6 minutes, with the Tekscan transducer interposed at the articulation.

3.2.4 Assessment of Porous Radial Head Implants

The results on the assessments of load magnitude and the viscoelastic response were used to establish the loading protocol (magnitude and time duration) for the effect of porosity on articular contact mechanics. The porous and solid hemiarthroplasty implants, and the native radial head were subjected to a uniaxial compressive load for 360 seconds at 4 frames per second (a total of 1440 frames of data) in each specimen. An initial ramp loading was applied over 3 seconds, after which the load was held constant at 150N. For each radial head construct, the contact area, maximum and mean and contact stress at the joint interface was collected for analysis at time t = 360 seconds during compressive loading.

3.2.5 Outcome Variables and Statistical Analysis for the Assessment of Radial Head Implants

Statistical analysis was performed using a repeated measures ANOVA test in SPSS Statistics software (IBM, Armonk, New York, USA). As mentioned, three (3) radial head models were tested against eleven (11) cadaveric specimens to investigate the effect of porosity on the contact area, and maximum contact stress experienced at the articulation of the radiocapitellar joint compared to a solid implant and the native radial head. A p-value of 0.05 was used to determine statistical significance in the results presented and were supported using an observed power of 0.8 and above.

3.3 Results

3.3.1 Effect of Load Magnitude

The relationship between the contact area at the articulation as load was increased from 0 – 200N is shown in Figure 3.2. The contact area rapidly increased upon initial load application followed by a gradual settling in contact area and finally, a plateau. The largest and most distinct increase in contact area of 90% occurred between 5 and 30 seconds where load reaches 100N. Contact area gradually settled between 100N and 150N increasing by 4%. Beyond 150N, results showed no change in contact area, except for a minor fluctuation, up to 170N, likely caused by the sensor.

An exponential relationship between the contact area and applied load was derived using the trends in the collected data where CA is contact area, and L is the applied load.

$$CA = 144 * [1 - Exp(-0.095 * L^{0.7})] \qquad \text{(Eq. 3.3)}$$

Eq. 3.3 was used to predict the expected contact area as load was increased past 150N. The equation revealed that even at an applied load of 400N, the contact area experienced at the articulation may only increase by approximately 3 ± 1 mm^2. Hence, it is rational to assume that testing at 150N results in outcome measurements that are stable over time.

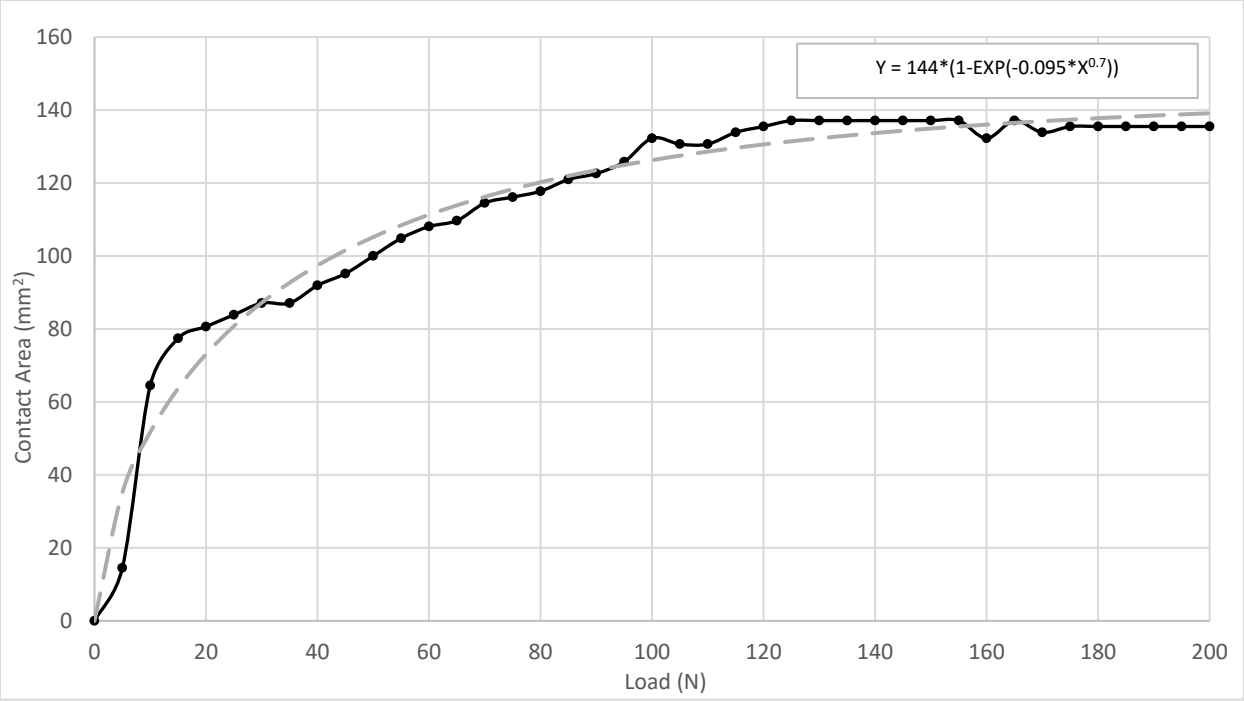

Figure 3.2 - The Effect of Incremental Load Application on Contact Area
The contact area at the hemiarthroplasty articulation is shown as load is incrementally increased from 0 – 200N. The grey dotted line represents the exponential relationship developed based on the data and the resulting equation is displayed above the trendline also given in Eq. 3.3.

3.3.2 Assessment of The Viscoelastic Response

Figure 3.3 shows representative plots of the change in (a) contact area and (b) maximum contact stress over time during constant uniaxial compression. There was a notable increase in contact area for both the native joint and hemiarthroplasty between times t = 3 seconds – where loading had reached equilibrium at 150N – and t = 360 seconds (p=0.001). At time t = 3 seconds, the average contact area for the native and hemiarthroplasty were 101 ± 34mm^2 and 86 ± 22mm^2 respectively and 157 ± 49mm^2 and 132 ± 42mm^2 respectively at time t = 360 seconds. On average, a 58 ± 30% and 56 ± 44% increase in contact area for the native and hemiarthroplasty radial heads, respectively occurred over the loaded interval. Conversely, the contact stress decreased over time, though this did not reach statistical significance (p = 0.063). The mean maximum contact stresses for the native

radial head and hemiarthroplasty at time t = 3 seconds and t = 360 seconds were 6.5 ± 2.5 MPa, 4.8 ± 2.0 MPa respectively and 5.3 ± 1.9 MPa, 4.9 ± 1.8 MPa respectively. The maximum contact stress decreased an average of 22 ± 20% and 8 ± 13% for the native joint and hemiarthroplasty respectively.

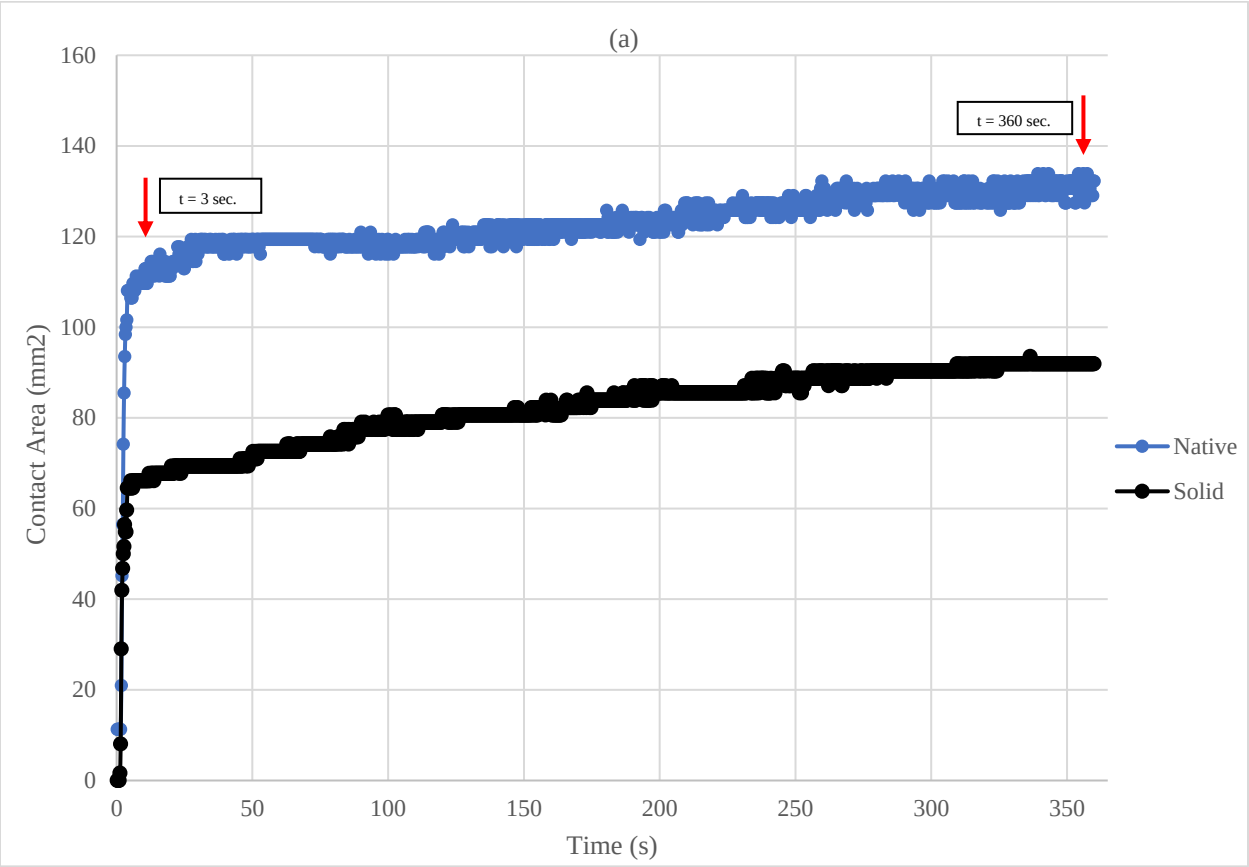

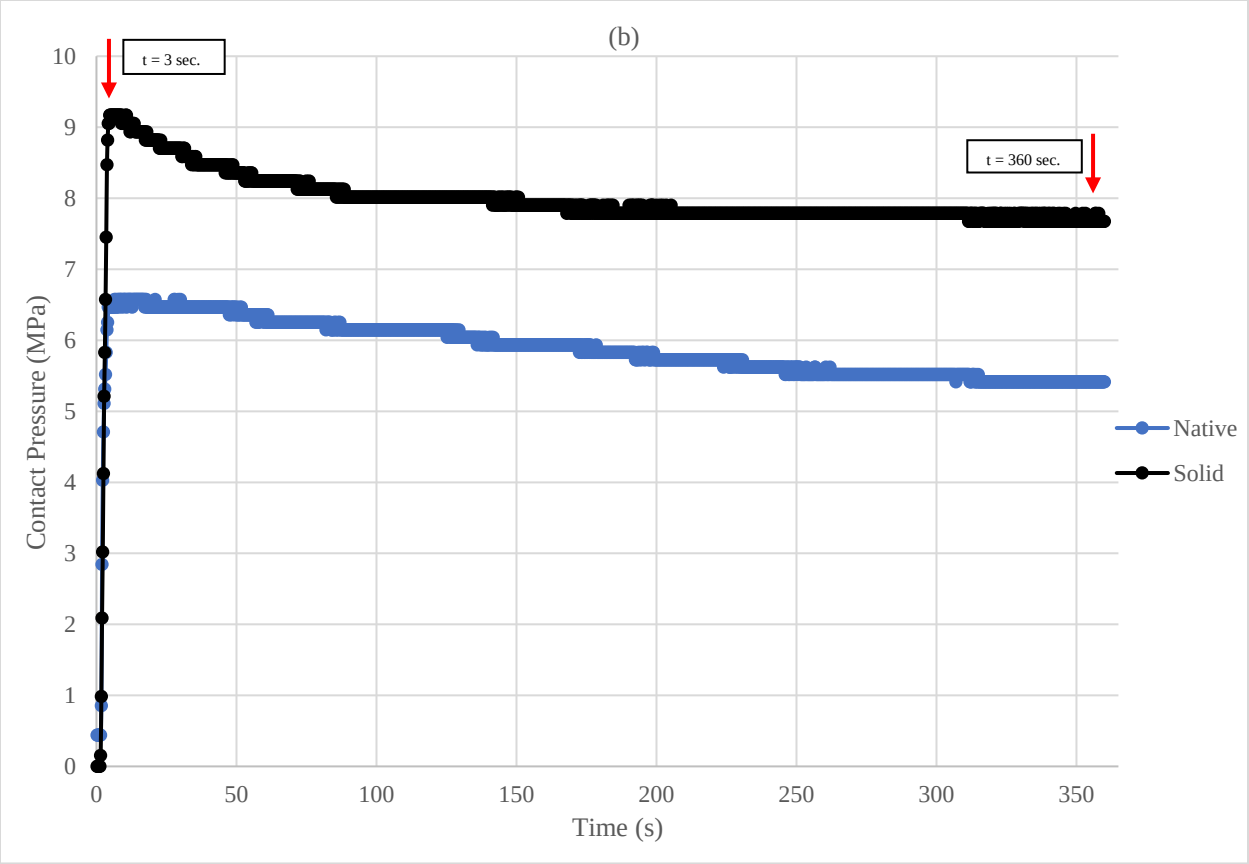

Figure 3.3 - The Effect of Time on (a) Contact Area and (b) Maximum Contact Stress
The blue and green data represents the native radial head and solid hemiarthroplasty respectively. Over a time-interval of 360 seconds, a plateauing effecting occurred indicating a combination of creep and stress relaxation effects to be considered in the evaluation of articular contact mechanics of hemiarthroplasty implants.

3.3.3 The Articular Contact Mechanics of Porous Radial Head Implants

Presented in this section are the contact stress distributions, the maximum contact stress and contact area results collected at time t = 360 seconds of the testing period.

3.3.3.1 Contact Stress Distributions

Figure 3.4 shows the contact stress distributions generated for a single specimen which represented the general trends in contact area and stress between the porous and solid hemiarthroplasty implants, and the native radial head. These profiles are significant in visualizing the changes in contact mechanics at the articulation as the porosity of the implants decreased from 80%-65%.

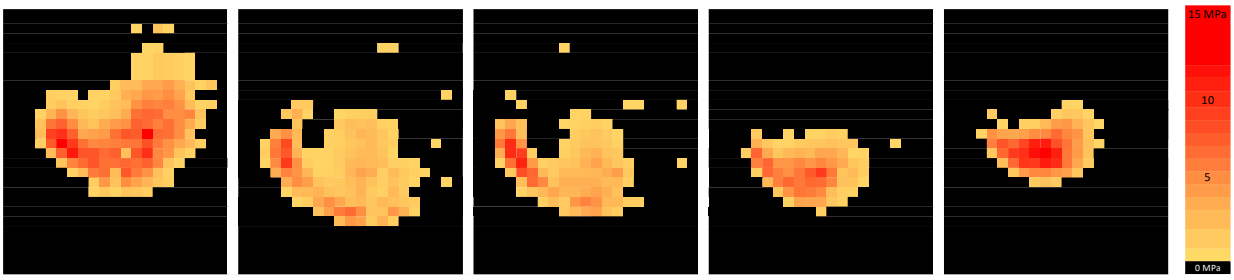

Figure 3.4 – Representative Contact Stress Distributions of the Native Radial Head, Porous and Solid Hemiarthroplasty Implants

The contact stress distributions were created using the data collected from the Tekscan Tactile sensor. Each profile is labeled with the respective percent porosities (in brackets) of each implant tested in the present study which correspond to internal strut diameter sizes of 0.4mm, 0.6mm, and 0.9mm.

The pressure profile of the native radial head shown in the above figure is very well distributed with maximum stresses occurring at the head's center. The large amounts of yellow represent very low stress levels. The increasing intensity of the colour gradient represents increasing stress levels where bright red is the maximum stress produced at the articulation. The size of the native pressure profile is also of significance. The number of highlighted sensels is typically highest for the native state and decreases as the internal strut diameter of the implants increase. The pressure profile of the solid radial head contains higher stress levels in concentrated areas. The pressure profiles for the three implants with porous internal lattice structures show a decrease in highlighted sensels and an increase in high stressed sensels as the porosity decreases from 80 – 65%. These profiles also show that in the porous hemiarthroplasties, stresses tend to concentrate around the edges of the implant becoming more centralized with decreasing porosity as in the contact pressure profiles of the native radial head and solid hemiarthroplasty implant.

3.3.3.2 Contact Area

The results for the contact area analysis are shown in Figure 3.5. There was a trend for the higher porosity implants (BCC4 & BCC6) to improve contact area similar to the native state, however, the results did not achieve statistical significance ($p = 0.261$). The native radial head produced the highest contact area which was 4.50 ± 237%, 3.93 ± 209%, 25.1 ± 152%, 15.8 ± 186% larger than the porous hemiarthroplasty implants with internal strut diameters of 0.4 mm, 0.6 mm, and 0.9mm and the solid hemiarthroplasty implant, respectively. The hemiarthroplasty with a 0.9mm internal strut diameter produced the lowest contact area of 25.1 ± 152%, of the native radial head. The power of this effect was only 0.273 likely due to the wide variation in contact measurements.

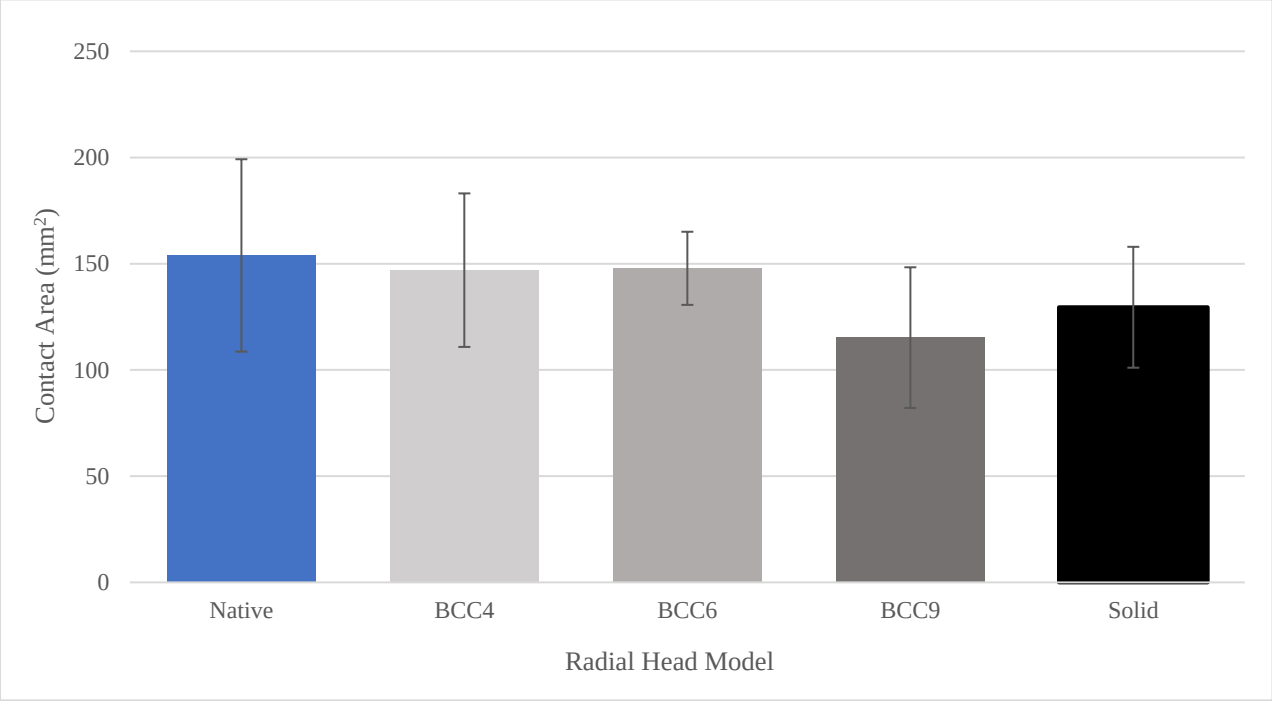

Figure 3.5 – Contact Area Results of the Porous and Solid Hemiarthroplasty Implants and the Native Radial Head at 150N

The implant models with internal strut diameters of 0.4mm, 0.6mm, and 0.9mm corresponded to porosities of 80%, 74%, and 65% respectively. The increasing intensity of the shading in three grey bars relates the increasing volume fraction of porosity.

3.3.3.3 Maximum Contact Stress

The results for the maximum contact stress analysis are show in Figure 3.6. There was a significant difference in maximum contact stress between the radial heads tested ($p = 0.001$) though there were no differences in contact stress between the three hemiarthroplasty implants with porous internal lattice structures ($p = 0.074$, $p = 0.564$). The porous radial head implant with an internal strut diameter equal to 0.4mm produced the lowest contact stress approximately 2.9 ± 0.9 MPa lower than the contact stresses produced by the native radial head. The native radial head produced the highest contact stresses approximately 58.1 ± 138%, 43.2 ± 133%, 47.7 ± 143% greater than the porous hemiarthroplasty implants with internal strut diameters of 0.4 mm, 0.6 mm, and 0.9mm, respectively. Significant differences between the native radial head and the solid hemiarthroplasty were not found producing mean differences equal to 0.1 ± 4.0 MPa under 150N of uniaxial compression ($p = 0.342$).

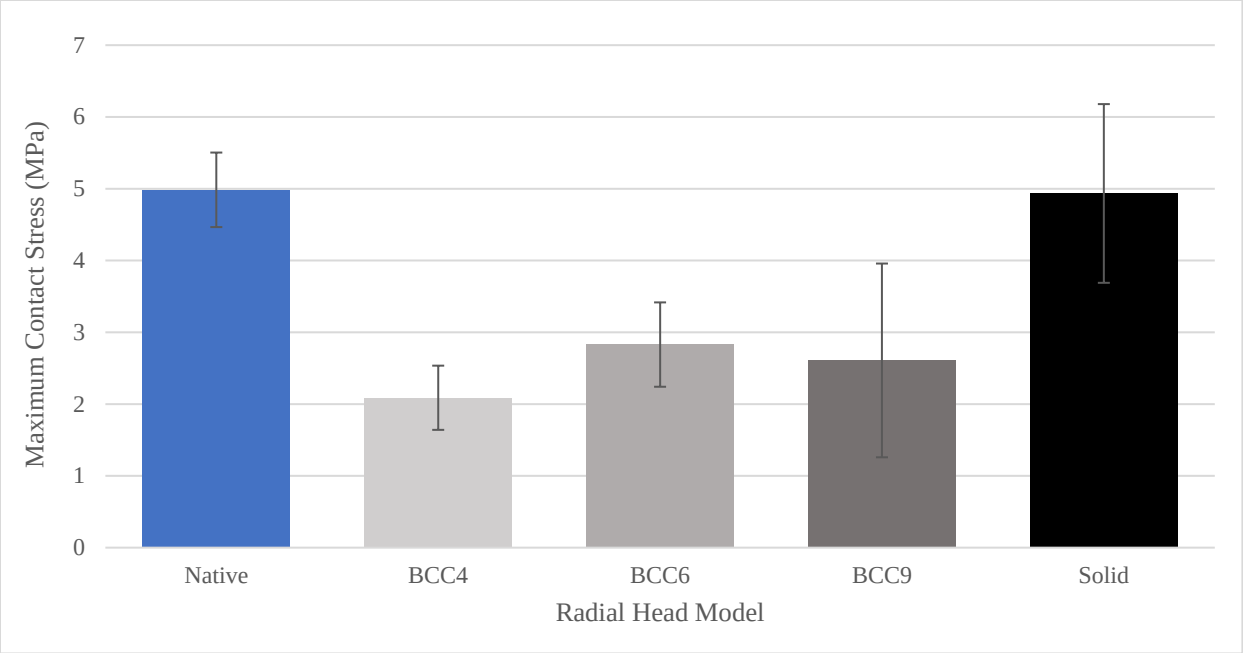

Figure 3.6 – Maximum Contact Stress Results of the Porous and Solid Hemiarthroplasty Implants and the Native Radial Head at 150N

The implant models with internal strut diameters of 0.4mm, 0.6mm, and 0.9mm corresponded to porosities of 80%, 74%, and 65% respectively. The increasing intensity of the shading in three grey bars relates the increasing volume fraction of porosity.

3.3.3.4 Mean Contact Stress

There were significant differences in the mean contact stress results, shown in Figure 3.7, for all of the radial head models assessed ($p = 0.001$) with the exception of the native radial head and solid hemiarthroplasty implant which produced mean contact stresses ($p = 0.323$). The three radial head models with porous internal lattice structures generated significantly different mean contact stresses ($p = 0.001$). The BCC4 model had the lowest mean contact stress, which increased by approximately 20 ± 200%, and 33 ± 200% as the internal strut diameter of the lattice increased in the BCC6, and BCC9 structures, respectively ($p = 0.02$, $p = 0.001$, respectively). Compared to the BCC4, BCC6, and BCC9 radial head constructs, the native radial head yielded a significantly higher mean contact stress 59 ± 82%, 55 ± 75%, and 35 ± 62% greater than the porous models, respectively. Finally, the results indicate that the BCC4, BCC6,

and BCC9 radial head models improved articular contact stress by approximately 42 ± 52%, 60 ± 70%, and 64 ± 62%, respectively compared to the solid model ($p = 0.001$).

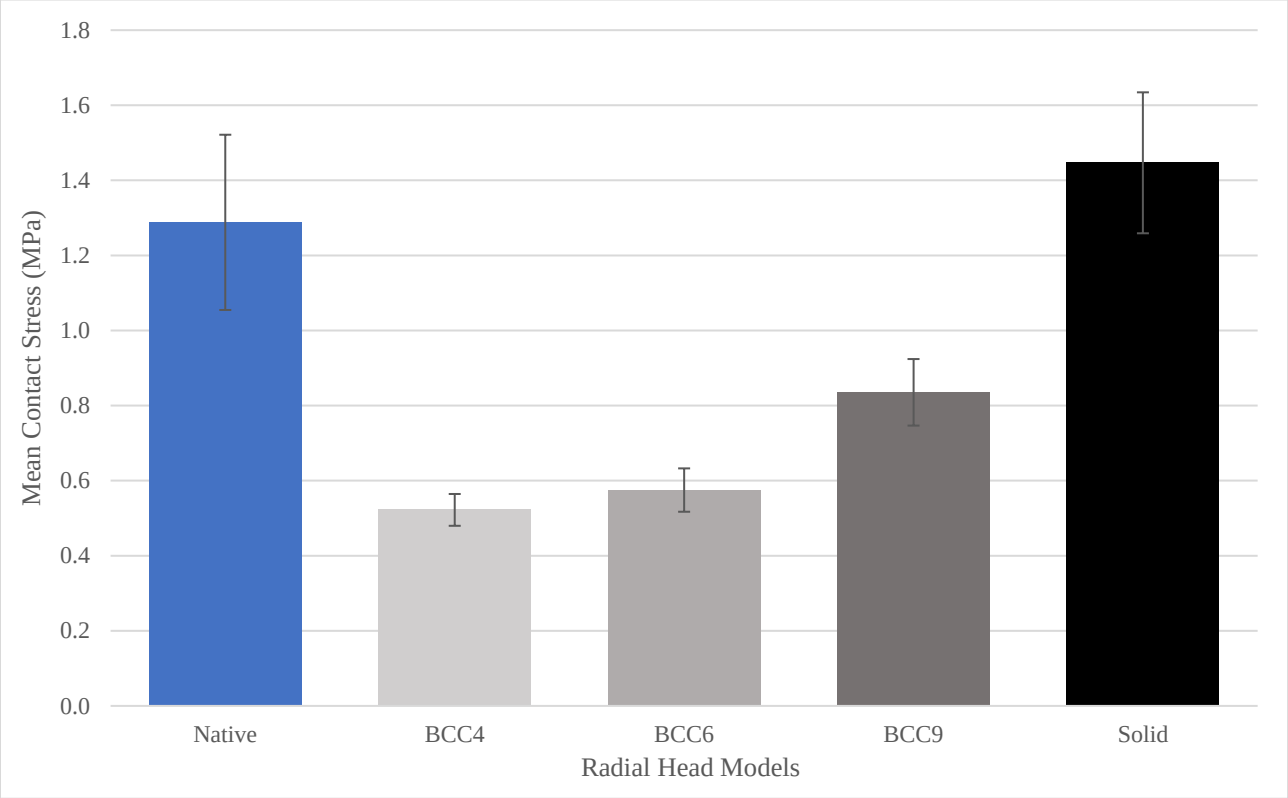

Figure 3.7 – Mean Contact Stress Results of the Porous and Solid Hemiarthroplasty Implants and the Native Radial Head at 150N

The implant models with internal strut diameters of 0.4mm, 0.6mm, and 0.9mm corresponded to porosities of 80%, 74%, and 65% respectively. The increasing intensity of the shading in three grey bars relates the increasing volume fraction of porosity.

3.4 Discussion

The Tekscan tactile sensor was chosen as the measurement tool for the present study as it provides real time contact data and contact pressure profiles allowing for in depth analysis of the joint contact mechanics. In a relatively dry environment, as used in the presented study, Tekscan yields consistent load output over time and hence the possibility of misinterpreting the results due to diminishing effects of the sensor was unlikely[84].

3.4.3 Implications on The Effective Modulus of Porous Hemiarthroplasty Implants

As described in **Chapter 2** of this thesis, the effective modulus of the porous hemiarthroplasty implants was approximated using the Nielsen Equation and the Gibson and Ashby Model. The effective modulus of the 80, 74, and 65% models were 79, 131, and 329 MPa, respectively and 76, 111, and 204 MPa, respectively. These values indicate increased discrepancy between the approximated moduli with decreasing porosity. Previous studies have used these models to evaluate the stiffness of additively manufactured BCC lattices. However, these approaches can not be used for comparison as different materials were used for construction herein. Our specimens were also encased in a thin solid shell which would have an important influence on the overall bulk stiffness of the implant.

The discrepancies between the two equation models may be explained by the geometric parameters of the lattice which contribute to the associated mechanical properties. The unit cell shape, size, and volume fraction of porosity used to construct a lattice will dictate the associated mechanical behaviour and the degree to which stiffness can be modified under various loading conditions. Geometric consideration becomes more important as porosity in the structure decreases via increasing strut diameter which thereby decreases pore size. Some level of geometric consideration was employed in the Neilson equation through the shape factor though the Gibson and Ashby

model evaluates the effective modulus based on the volume fraction alone. These theoretical models provide a good approximation of the expected stiffness reduction; however, future work should include experimental or computational evaluation of the porous structures to evaluate the mechanical properties more adequately.

3.4.1 Assessment of Load Magnitude

These investigations demonstrated a relative plateauing effect in the observed contact area occurring at approximately 100-150N with some minor fluctuation, as was shown in Figure 3.3. As such 150N was used for the subsequent testing. An applied load beyond 150N would likely cause little change in the measured contact area. This was shown via a combination of the data trends and the approximated contact area using Eq. 3.3. The elbow joint experiences significant compressive forces that can be as large as 3x the human body weight. The radiocapitellar joint can transmit up to 60% of the total force thus making 150N a suitable and clinically relevant load magnitude for experimental testing.

3.4.2 The Effect of The Viscoelastic Response on Articular Contact Mechanics

The results of this investigation show a significant change in contact area over time. While significance was not achieved for contact stress, the trends in the maximum contact stress were identical to those in the contact area results indicating a stress relaxation behaviour in the cartilage as each implant was held under a constant 150N load over a 6-minute testing period. This is likely because cartilage experiences an almost immediate elastic response to the application of compressive load. After which, cartilage follows an asymptotic response continuing to deform over time due to the dynamic movement of the fluid phase (as demonstrated in Figure 3.4), a behaviour commonly referred to as a creep response. Movement of the fluid layer becomes more difficult with the added compression thus taking longer to reach biomechanical equilibrium hence

the importance of performing experimental analysis over time. The native radiocapitellar articulation also contains a second layer of protective cartilaginous tissue that hemiarthroplasty implants do not have which would explain the higher magnitudes of contact area generated by the native radial head. Lawless et al., conducted a study on the viscoelasticity of articular cartilage and suggests that under low stress levels cartilage behaves in a more "viscous" manner and under higher stresses cartilage experiences more "elastic" behaviour[40,41]. The movement of the fluid layer allows for increased contact between the radial head and the capitellum however, the viscous behaviour of the fluid phase is also partially responsible for resisting applied load which may explain higher magnitudes of contact stress compared to other academic works which did not consider time or viscoelasticity as a contributing factor.

While further investigation is needed, these findings suggest that due to the viscoelastic properties of cartilage, there is a relative plateauing effect in the articular biomechanics of the joint when loaded over time. Other concave-convex articulations like the knee and hip can be subject to long compressive loads while standing, walking, or running for extended periods of time. As such it is important to consider viscoelasticity during mechanical and computational modeling of articulations in future work.

3.4.4 The Articular Contact Mechanics of Porous Radial Head Implants

Pressure profiles for the porous and solid hemiarthroplasty implants, along with the native radial head at time t = 360s were analyzed. Visual inspection of the images in Figure 3.5 suggests an increase in contact area and decrease in contact stress as the porosity of the implant increases. The contact maps of the native joint and solid hemiarthroplasty implant are similar such that maximum stress occurs at the center of the radial head though the porous implants with BCC lattice structures of varying internal strut diameters experience maximum stress values at the outer edges of the

implant. The stresses may be explained by the behaviour of the internal lattice structure such that the struts of the lattice relieve stress from the center of the radial head by way of bending in response to the compressive load. In doing so, the edges of the porous hemiarthroplasty implants become raised or sharpened, thus increasing the stress in these locations. A common pattern of high stress was recognized on the lateral edges of the porous implants. The effects of the sharpened edges may have been exacerbated by compression against the capitellum and alleviated due to the concave nature of the trochlearcapitellar groove.

3.4.4.1 The Effect of Porosity on Contact Area

The more porous BCC4 and BCC6 hemiarthroplasty implants did produce some improvement in the contact area and approached the native state, although significant differences were not achieved. This finding is encouraging as it suggests that the porous hemiarthroplasty implants with internal lattice structures may in fact be able to produce contact mechanics similar to the native state. The solid UHMWPE hemiarthroplasty tended to reduce contact area relative to the native radial head. These results align with those found by Berkmortel et al., investigating the effect of material on hemiarthroplasty implant compliance[7]. In addition to the mechanics of the porous structure and the influence on articular mechanics, the concave nature of the implant may also play a role. Membrane stresses (i.e. the uniform distribution of the applied load over a surface area) develop in the concave surface when loaded which increases strength and stiffness as well as resistance to deformation[7]. Further design alterations and studies are needed to consider this aspect of the design.

3.4.4.2 The Effect of Porosity on Contact Stress

Implementing a porous internal lattice structure in radial head implants decreased both maximum and mean contract stress at the articulation. The mean contact stress results show a significant decrease with increasing porosity and although there was a trend for lower stresses with higher porosity, no significant differences in maximum contact stress were found between the 80%, 74%, and 65% porous implants (*viz.* BCC4, BCC6, BCC9). The combined results for maximum and mean contact stress suggest that an internal structural lattice design can effectively improve the contact mechanics of a radial head hemiarthroplasty as compared to a solid implant with identical geometry and similar material properties. These results are likely a product of two factors: (1) the reduction in effective stiffness and (2) the unique mechanical properties of lattice structures. As per the Nielsen Equation and the Gibson and Ashby model, the theoretical effective moduli of the porous implants were well below the stiffness threshold of ~300 MPa suggested in previous work[3,7,27] (Table 3.1). The BCC9 radial head model was the only exception when approximated using the Nielsen equation predicting an effective modulus of 330 MPa. Theoretical evaluations of mechanical properties such as the Nielsen Equation and the Gibson and Ashby Model have been shown to yield lower stiffness values compared to a computational or experimental evaluation alluding to the possibility that the porous structures may have been stiffer than the suggested threshold. As such, the significant reduction in maximum and mean contact stresses for the porous implants may also be attributed to the internal lattice structure providing additional structural flexibility and advanced energy absorbing capabilities. In solid implant models, load is dissipated across the area of the articulating surface, however, the lattice allows for further dissipation of the load through the struts of the lattice. Previous studies on the specific energy absorbing (SEA) capabilities of lattice structures have recognized the BCC lattice for its exceptional energy absorbing capabilities compared to other lattice designs. This can be attributed to the bending-

dominated nature of the structure allowing substantial amounts of energy, imposed by a constant compressive load, to be stored in the lattice struts[85,86]. The SEA of a lattice can be even further optimized using geometric modifications to the unit cell.

Lattice structures have impressive strength and stiffness properties though buckling failure of the internal struts was a prominent concern in conducting this work. With no significant differences in maximum contact stress between the three porous hemiarthroplasty implants, it is fair to suggest that larger strut diameters such as 0.9mm would generate the desired implant stiffness to reduce articular cartilage wear and significantly reduce the threat of loading failure. For a better understanding, further investigation on the strength and fatigue properties of the tested structures is needed.

The native radial head produced similar maximum contact stresses to the solid hemiarthroplasty implant. UHMWPE has a considerably lower Young's modulus compared to commonly used metal implant materials, though previous findings have reported no significant differences in contact stress relative to metal. It was therefore expected that the native radial head would perform significantly better than a solid implant generating significantly lower mean and maximum contact stresses, however this was not the case[7]. A 2001 study reported that articular cartilage will begin to experience apoptosis when under stress levels above 5 MPa[87]. While none of the porous or solid hemiarthroplasty implants produced such contact stresses, the native radial head produced rather high and unexpected contact stresses between 1 – 10 MPa during the 6-minute testing period. The mean maximum contact pressure for the native state was approximately 4.9 ± 2.1 MPa at 150N. Such stress levels may be explained by possible tissue dehydration, testing at room temperature versus body temperature, and that the cadaveric specimens had been preserved in a freezer which may have altered the tissue properties. All cadaveric specimens were screened for any significant

osteoarthritis or cartilage damage however, minor inconsistencies in the morphology of the radial head/dish including a non-spherical shape, and/or small asperities, surface pitting or scratches could have also led to localized high stresses (which were reported herein as peak stresses) in the native state.

Since the contact area for the native state was greater than the implants assessed, it is logical to postulate that overall, the average stresses were lower, save for these peaks. This was in some ways confirmed by the contact stress results for the native radial head where the mean contact stress was approximately 75 ± 100% lower than the reported peak stresses. The native radial head also generated lower mean contact stresses than the solid hemiarthroplasty though this finding did not reach significance. Further analysis of the mean and maximum contact stress results for the native radial head may allude to malrotation and malalignment of the specimens during testing resulting in high native stresses. Proper positioning of the articulating surfaces is increasingly important with respect to the native radial head as it is non-axisymmetric and hence more susceptible to malalignment then are axisymmetric models. Langhor et al., conducted a study in this regard whose results show high sensitivity to rotational positioning up to 21% in the native articulation. Furthermore, their findings suggest that implant asymmetry increases susceptibility to the impingement phenomena – abnormal contact between the articulating surfaces – which may explain atypical contact stresses results in the native radial head compared to the porous and solid implants assessed which were axisymmetric[50].

Previous computational and experimental work on articular biomechanics of hemiarthroplasty implants have not found similar findings with respect to contact stress, and in fact demonstrated that the native state produced optimal contact mechanics with respect to both contact area and contact stress in the assessment of alternative radial head hemiarthroplasty materials and geometric

design parameters. The reduction in contact stress of the porous implants compared to the native radial head could also be attributed to the low modulus of PA2200 which may have provided increased flexibility in response to load.

3.5 Conclusion

The viscoelastic response has demonstrated significant implications on the biomechanical behaviour of hemiarthroplasty implants over time suggesting an average increase in contact area of 58% and 56% for the native and solid radial heads, respectively over a 6-minute interval. The viscoelastic properties of articular cartilage should be considered in investigations of articular biomechanics to adequately apply the presented findings to other convex-concave articulations that undergo extended periods of compressive loading.

The present study demonstrates the efficacy of a porous internal lattice structure in improving articular biomechanics of the radiocapitellar joint. The effective moduli of the implants with a porous internal lattice structure were approximated by Gibson and Ashby model and the Nielsen Equation which suggest an 80-90% decrease in effective stiffness of the porous implants compared to the solid implant. Despite no significant improvements in the contact area amongst the porous and solid hemiarthroplasty implants and the native radial head, the porous implants showed improvements in mean and maximum contact stresses compared to the solid implant. Future research should investigate alternative loading conditions to understand the long-term capabilities of these structures including a wider spectrum of porosities and lattice geometries to provide further insight on the effects of porous hemiarthroplasty implants on articular contact mechanics.

3.6 References

1. Lavrenko PN, Raglis V V. *Automatic Cassette Diffusometer*. Vol 29.; 1986.

2. Pt TLU, Therapy P, Second S. Hemiarthroplasty Total Shoulder Arthroplasty Imaging of Total Joint Replacement. 2018.

3. Dedecker S. The Efficacy of Bionate as an Articulating Surface for Joint Hemiarthroplasty. 2017;(January):1-85.

4. Bleß HH, Kip M. White paper on joint replacement: Status of hip and knee arthroplasty care in Germany. *White Pap Jt Replace Status Hip Knee Arthroplast Care Ger*. 2017:1-135. doi:10.1007/978-3-662-55918-5

5. Arthritis Foundation. Arthritis by the Numbers. *Arthritis Found*. 2019:1-70. https://www.arthritis.org/getmedia/e1256607-fa87-4593-aa8a-8db4f291072a/2019-abtn-final-march-2019.pdf.

6. Pappas N, Bernstein J. Fractures in brief: Radial head fractures. *Clin Orthop Relat Res*. 2010;468(3):914-916. doi:10.1007/s11999-009-1183-1

7. Berkmortel C. Lower Stiffness Orthopaedic Implants for Hemiarthroplasty. 2020:130.

8. Lizhang J, Fisher J, Jin Z, Burton A, Williams S. The effect of contact stress on cartilage friction, deformation and wear. *Proc Inst Mech Eng Part H J Eng Med*. 2011;225(5):461-475. doi:10.1177/2041303310392626

9. Einhorn TA, Guy- G, Schemitsch EH, et al. new england journal. 2019:2199-2208. doi:10.1056/NEJMoa1906190

10. Robertson GAJ, Wood AM, Wood AM. Hip hemi-arthroplasty for neck of femur fracture : What is the current evidence ? 2018;9(11):235-244. doi:10.5312/wjo.v9.i11.235

11. Jr DJH, Hsu JE, Iii FAM. Primary Shoulder Hemiarthroplasty : What Can Be Learned From 359 Cases That Were Surgically Revised ? 2018:1031-1040. doi:10.1007/s11999.0000000000000167

12. Wagner ER, Farley KX, Higgins I, Wilson JM, Daly CA, Gottschalk MB. The incidence of shoulder arthroplasty : rise and future projections compared with hip and knee arthroplasty. *J Shoulder Elb Surg*. 2020;29(12):2601-2609. doi:10.1016/j.jse.2020.03.049

13. Trofa D, Rajaee SS, Smith EL. Nationwide Trends in Total Shoulder Arthroplasty and Hemiarthroplasty for Osteoarthritis. 2014;(April):166-172.

14. Bekerom MPJ Van Den, Geervliet PC, Somford MP, Den MPJ Van. Original Article Total shoulder arthroplasty versus hemiarthroplasty for glenohumeral arthritis : A systematic review of the literature at long-term follow-up. 2013;7(3):3-8. doi:10.4103/0973-6042.118915

15. Gezeral OS. Prosthesis arthritis toronto,. :244-255.

16. Mccann LÃ, Ingham E, Jin Z, Fisher J. An investigation of the effect of conformity of knee hemiarthroplasty designs on contact stress , friction and degeneration of articular cartilage : A tribological study. 2009;42:1326-1331. doi:10.1016/j.jbiomech.2009.03.028

17. Vance MC, Wolfe SW, Packer G, Tan D, Crisco JJT, Ph D. Midcarpal Hemiarthroplasty for Wrist Arthritis : Rationale and Early Results. 2012;1(212):61-67.

18. Anneberg M, Packer G, Crisco JJ, Wolfe S. Four-Year Outcomes of Midcarpal Hemiarthroplasty for Wrist Arthritis. *J Hand Surg Am*. 2017;42(11):894-903. doi:10.1016/j.jhsa.2017.07.029

19. Jr EGH, Lum Z, Bamberger HB, Trzeciak MA. Failure of Wrist Hemiarthroplasty. 2017. doi:10.1177/1558944716668836

20. Rticle CRA, Beasley J. FOR Osteoarthritis and Rheumatoid Arthritis : Conservative Therapeutic Management. *J Hand Ther*. 2012;25(2):163-172. doi:10.1016/j.jht.2011.11.001

21. Pettersson K, Amilon A, Rizzo M. Pyrolytic Carbon Hemiarthroplasty in the Management of Proximal Interphalangeal Joint Arthritis. *J Hand Surg Am*. 2015;40(3):462-468. doi:10.1016/j.jhsa.2014.12.016

22. Hohman DW, Nodzo SR, Qvick LM, Duquin TR, Paterson PP. Hemiarthroplasty of the distal humerus for acute and chronic complex intra-articular injuries. *J Shoulder Elb Surg*. 2014;23(2):265-272. doi:10.1016/j.jse.2013.05.007

23. Stuffmann E, Baratz ME. Radial Head Implant Arthroplasty. *YJHSU*. 2009;34(4):745-754. doi:10.1016/j.jhsa.2009.01.027

24. Estrada-Malacón CA, Pérez-Valtierra M, Torres-Zavala A, Fonseca-Bernal M. Hemiartroplastía de cúpula radial en pacientes con fractura tipo III y IV según Mason Johnston. *Acta ortopédica Mex*. 2015;29(3):148-154.

25. Kodde IF, Kaas L, Flipsen M, Bekerom MPJ Van Den, Eygendaal D. Current concepts in the management of radial head fractures. 2015;6(11):954-960. doi:10.5312/wjo.v6.i11.954

26. Phadnis J, Watts AC, Bain GI. Elbow hemiarthroplasty for the management of distal humeral fractures: current technique, indications and results. *Shoulder Elb*. 2016;8(3):171-183. doi:10.1177/1758573216640210

27. Khayat A. Effect of Hemiarthroplasty Implant Contact Geometry and Material on Early Cartilage Wear. 2015;(October):1-102.

28. Sahu D, Holmes DM, Fitzsimmons JS, et al. Influence of radial head prosthetic design on radiocapitellar joint contact mechanics. *J Shoulder Elb Surg*. 2014;23(4):456-462. doi:10.1016/j.jse.2013.11.028

29. Dumas M, Terriault P, Brailovski V. Modelling and characterization of a porosity graded lattice structure for additively manufactured biomaterials. *Mater Des*. 2017;121:383-392. doi:10.1016/j.matdes.2017.02.021

30. Disc I, Ligament AC, Tis- B, Bone C, Remodeling B. Learn more about Stress Shielding Responses of Musculoskeletal Tissues to Disuse and Remobilization. 2014.

31. Krishna BV, Bose S, Bandyopadhyay A. Low stiffness porous Ti structures for load-bearing implants. *Acta Biomater*. 2007;3(6):997-1006. doi:10.1016/j.actbio.2007.03.008

32. Matassi F, Botti A, Sirleo L, Carulli C, Innocenti M. Porous metal for orthopedics implants. *Clin Cases Miner Bone Metab*. 2013;10(2):111-115. doi:10.11138/ccmbm/2013.10.2.111

33. Arabnejad S, Johnston B, Tanzer M, Pasini D. Fully porous 3D printed titanium femoral stem to reduce stress-shielding following total hip arthroplasty. *J Orthop Res*. 2017;35(8):1774-1783. doi:10.1002/jor.23445

34. Chanlalit C, Shukla DR, Fitzsimmons JS, An KN, O'Driscoll SW. Stress Shielding Around Radial Head Prostheses. *J Hand Surg Am*. 2012;37(10):2118-2125. doi:10.1016/J.JHSA.2012.06.020

35. Jin H, Lewis JL. Determination of Poisson's Ratio of Articular Cartilage by Indentation Using Different-Sized Indenters. *J Biomech Eng*. 2004;126(2):138-145. doi:10.1115/1.1688772

36. Sophia Fox AJ, Bedi A, Rodeo SA. The basic science of articular cartilage: Structure, composition, and function. *Sports Health*. 2009;1(6):461-468. doi:10.1177/1941738109350438

37. Cruess RL, Kwok DC, Duc PN, Lecavalier MA, Dang GT. The response of articular cartilage to weight-bearing against metal. A study of hemiarthroplasty of the hip in the dog. *J Bone Jt Surg - Ser B*. 1984;66(4):592-597. doi:10.1302/0301-620x.66b4.6204988

38. Chan SMT, Neu CP, Komvopoulos K, Reddi AH, Di Cesare PE. Friction and wear of hemiarthroplasty biomaterials in reciprocating sliding contact with articular cartilage. *J Tribol*. 2011;133(4). doi:10.1115/1.4004760

39. Schwartz CJ, Bahadur S. Investigation of articular cartilage and counterface compliance in multi-directional sliding as in orthopedic implants. 2007;262:1315-1320. doi:10.1016/j.wear.2007.01.007

40. Lawless BM, Sadeghi H, Temple DK, Dhaliwal H, Espino DM, Hukins DWL. Viscoelasticity of articular cartilage: Analysing the effect of induced stress and the restraint of bone in a dynamic environment. *J Mech Behav Biomed Mater*. 2017;75(May):293-301. doi:10.1016/j.jmbbm.2017.07.040

41. Katta J, Jin Z, Ingham E, Fisher J. Biotribology of articular cartilage-A review of the

recent advances. *Med Eng Phys*. 2008;30(10):1349-1363. doi:10.1016/j.medengphy.2008.09.004

42. Oungoulian SR, Durney KM, Jones BK, Ahmad CS, Hung CT, Ateshian GA. Wear and damage of articular cartilage with friction against orthopedic implant materials. *J Biomech*. 2015;48(10):1957-1964. doi:10.1016/j.jbiomech.2015.04.008

43. Fornalski S, Lee TQ. Anatomy and Biomechanics of the Elbow Joint. 2003;7(4):168-178.

44. Kvist J, Thomeé R. *Structured Rehabilitation Model with Clinical Outcomes After ACL Reconstruction*.; 2014. doi:10.1007/978-3-642-36801-1

45. Batlle JA, Cerezal L, Dolores M, et al. The elbow : review of anatomy and common collateral ligament complex pathology using MRI. 2019;7.

46. Contact Stress Analysis of the Elbow Joint ; Design of Radial Head Replacements. *Clin Orthop*. 2011;(567):2011-2011.

47. Langohr GDG, Willing R, Medley JB, King GJW, Johnson JA. The Effect of Radial Head Hemiarthroplasty Geometry on Proximal Radioulnar Joint Contact Mechanics. *J Hand Surg Am*. 2016;41(7):745-752. doi:10.1016/j.jhsa.2016.05.001

48. Shannon HL. The Contact Mechanics and Kinematics of Radial Head Implants. 2012;Master of(Paper 745):60-66. http://ir.lib.uwo.ca/etd/745.

49. Irish SE, Langohr GDG, Willing R, King GJ, Johnson JA. Implications of radial head hemiarthroplasty dish depth on radiocapitellar contact mechanics. *J Hand Surg Am*. 2015;40(4):723-729. doi:10.1016/j.jhsa.2015.01.030

50. Langohr GDG, Willing R, Medley JB, Johnson JA, King GJW. The Effect of Radial Head Hemiarthroplasty Geometry on Radiocapitellar Joint Contact Mechanics. *J Shoulder Elb Surg*. 2015;24(4):e118. doi:10.1016/j.jse.2014.11.024

51. van Grunsven W, Hernandez-Nava E, Reilly G, Goodall R. Fabrication and Mechanical Characterisation of Titanium Lattices with Graded Porosity. *Metals (Basel)*. 2014;4(3):401-409. doi:10.3390/met4030401

52. De LMR. Evaluation of bone ingrowth into porous titanium implant : histomorphometric analysis in rabbits. 2010;24(4):399-405.

53. Rahimizadeh A, Nourmohammadi Z, Arabnejad S, Tanzer M, Pasini D. Porous architected biomaterial for a tibial-knee implant with minimum bone resorption and bone-implant interface micromotion. *J Mech Behav Biomed Mater*. 2018;78(November 2017):465-479. doi:10.1016/j.jmbbm.2017.11.041

54. Yan C, Hao L, Hussein A, Raymont D. Evaluations of cellular lattice structures manufactured using selective laser melting. *Int J Mach Tools Manuf*. 2012;62:32-38. doi:10.1016/j.ijmachtools.2012.06.002

55. Pan C, Han Y, Lu J. Design and optimization of lattice structures: A review. *Appl Sci*. 2020;10(18):1-36. doi:10.3390/APP10186374

56. Obadimu SO, Kourousis KI. Compressive behaviour of additively manufactured lattice structures: A review. *Aerospace*. 2021;8(8). doi:10.3390/aerospace8080207

57. Abd Malek NMS, Mohamed SR, Che Ghani SA, Wan Harun WS. Critical evaluation on structural stiffness of porous cellular structure of cobalt chromium alloy. *IOP Conf Ser Mater Sci Eng*. 2015;100(1). doi:10.1088/1757-899X/100/1/012019

58. Hazlehurst K, Wang CJ, Stanford M. Evaluation of the stiffness characteristics of square pore CoCrMo cellular structures manufactured using laser melting technology for potential orthopaedic applications. *Mater Des*. 2013;51:949-955. doi:10.1016/j.matdes.2013.05.009

59. Wang L, Kang J, Sun C, Li D, Cao Y, Jin Z. Mapping porous microstructures to yield desired mechanical properties for application in 3D printed bone scaffolds and orthopaedic implants. *Mater Des*. 2017;133:62-68. doi:10.1016/j.matdes.2017.07.021

60. Choren JA, Heinrich SM, Silver-Thorn MB. Young's modulus and volume porosity relationships for additive manufacturing applications. *J Mater Sci*. 2013;48(15):5103-5112. doi:10.1007/s10853-013-7237-5

61. Tapscott DC, Wottowa C. Orthopedic Implant Materials. *StatPearls*. July 2021. https://www.ncbi.nlm.nih.gov/books/NBK560505/. Accessed November 24, 2021.

62. Mehboob H, Tarlochan F, Mehboob A, Chang SH. Finite element modelling and characterization of 3D cellular microstructures for the design of a cementless biomimetic porous hip stem. *Mater Des*. 2018;149:101-112. doi:10.1016/j.matdes.2018.04.002

63. Luxner MH. Numerical simulations of 3D open cell structures – influence of structural irregularities on elasto-plasticity and deformation localization. 2007;44:2990-3003. doi:10.1016/j.ijsolstr.2006.08.039

64. Parthasarathy J, Starly B, Raman S, Christensen A. Mechanical evaluation of porous titanium (Ti6Al4V) structures with electron beam melting (EBM). *J Mech Behav Biomed Mater*. 2010;3(3):249-259. doi:10.1016/j.jmbbm.2009.10.006

65. Limmahakhun S, Oloyede A, Sitthiseripratip K, Xiao Y, Yan C. 3D-printed cellular structures for bone biomimetic implants. *Addit Manuf*. 2017;15:93-101. doi:10.1016/j.addma.2017.03.010

66. Yan C, Hao L, Hussein A, Bubb SL, Young P, Raymont D. Evaluation of light-weight AlSi10Mg periodic cellular lattice structures fabricated via direct metal laser sintering. *J Mater Process Technol*. 2014;214(4):856-864. doi:10.1016/j.jmatprotec.2013.12.004

67. Wendy Gu X, Greer JR. Ultra-strong architected Cu meso-lattices. *Extrem Mech Lett*. 2015;2(1):7-14. doi:10.1016/j.eml.2015.01.006

68. Tao W, Leu MC. Design of lattice structure for additive manufacturing. *Int Symp Flex Autom ISFA 2016*. 2016;(November 2018):325-332. doi:10.1109/ISFA.2016.7790182

69. Tancogne-Dejean T, Spierings AB, Mohr D. Additively-manufactured metallic micro-lattice materials for high specific energy absorption under static and dynamic loading. *Acta Mater*. 2016;116:14-28. doi:10.1016/j.actamat.2016.05.054

70. Hailu YM, Nazir A, Lin SC, Jeng JY. The effect of functional gradient material distribution and patterning on torsional properties of lattice structures manufactured using multijet fusion technology. *Materials (Basel)*. 2021;14(21):1-21. doi:10.3390/ma14216521

71. Soltani-Tehrani A, Lee S, Sereshk MRV, Shamsaei N. Effects of unit cell size on the mechanical performance of additive manufactured lattice structures. *Solid Free Fabr 2019 Proc 30th Annu Int Solid Free Fabr Symp - An Addit Manuf Conf SFF 2019*. 2019:2254-2262.

72. Jetté B, Brailovski V, Dumas M, Simoneau C, Terriault P. Femoral stem incorporating a diamond cubic lattice structure: Design, manufacture and testing. *J Mech Behav Biomed Mater*. 2018;77(August 2017):58-72. doi:10.1016/j.jmbbm.2017.08.034

73. Heinl P, Müller L, Körner C, Singer RF, Müller FA. Cellular Ti-6Al-4V structures with interconnected macro porosity for bone implants fabricated by selective electron beam melting. *Acta Biomater*. 2008;4(5):1536-1544. doi:10.1016/j.actbio.2008.03.013

74. Hazlehurst KB, Wang CJ, Stanford M. A numerical investigation into the influence of the properties of cobalt chrome cellular structures on the load transfer to the periprosthetic femur following total hip arthroplasty. *Med Eng Phys*. 2014;36(4):458-466. doi:10.1016/j.medengphy.2014.02.008

75. Kodir K, Tanti I, Odang RW, Shulpekov AM, Kashapov LN, Kashapov NF. Critical evaluation on structural stiffness of porous cellular structure of cobalt chromium alloy Critical evaluation on structural stiffness of porous cellular structure of cobalt chromium alloy. 2015. doi:10.1088/1757-899X/100/1/012019

76. Gibson LJ, Editor G. C ellular Solids. 2021;(APRIL 2003):270-274.

77. Fuglsang Nielsen L. Elasticity and damping of porous materials and impregnated materials. *J Am Ceram Soc*. 1983;67:93-98.

78. Head R. EVOLVE Proline Plus Radial Head and Repair System.

79. Pereira TF, Oliveira MF, Maia IA, Silva JVL, Costa MF, Thiré RMSM. 3D printing of poly(3-hydroxybutyrate) porous structures using selective laser sintering. *Macromol Symp*. 2012;319(1):64-73. doi:10.1002/masy.201100237

80. Savalani MM, Hao L, Zhang Y, Tanner KE, Harris RA. Fabrication of porous bioactive structures using the selective laser sintering technique. *Proc Inst Mech Eng Part H J Eng*

Med. 2007;221(8):873-886. doi:10.1243/09544119JEIM232

81. Mazzoli A. Selective laser sintering in biomedical engineering. *Med Biol Eng Comput*. 2013;51(3):245-256. doi:10.1007/s11517-012-1001-x

82. Chin HC, Khayat G, Quinn TM. Improved characterization of cartilage mechanical properties using a combination of stress relaxation and creep. *J Biomech*. 2011;44(1):198-201. doi:10.1016/j.jbiomech.2010.09.006

83. Lanting BA, Ferreira LM, Johnson JA, King GJ, Athwal GS. Clinical Biomechanics Radial head implant diameter : A biomechanical assessment of the forgotten dimension. *JCLB*. 2015;30(5):444-447. doi:10.1016/j.clinbiomech.2015.03.012

84. Jansson KS, Michalski MP, Smith SD, LaPrade RF, Wijdicks CA. Tekscan pressure sensor output changes in the presence of liquid exposure. *J Biomech*. 2013;46(3):612-614. doi:10.1016/j.jbiomech.2012.09.033

85. Tancogne-Dejean T, Mohr D. Stiffness and specific energy absorption of additively-manufactured metallic BCC metamaterials composed of tapered beams. *Int J Mech Sci*. 2018;141(February):101-116. doi:10.1016/j.ijmecsci.2018.03.027

86. Zhao M, Liu F, Fu G, Zhang DZ, Zhang T, Zhou H. Improved mechanical properties and energy absorption of BCC lattice structures with triply periodic minimal surfaces fabricated by SLM. *Materials (Basel)*. 2018;11(12). doi:10.3390/ma11122411

87. Thibault M, Poole AR, Buschmann MD. Cyclic compression of cartilage / bone explants in vitro leads to physical weakening , mechanical breakdown of collagen and release of matrix fragments. 2002;20:1265-1273.

Chapter 4

4 Conclusion

This chapter summarizes the work completed within this thesis and the key findings. Also discussed, are the strengths and limitations of the presented work, recommendations for future work, and final conclusions.

4.1 Summary of Work

The presented work was conducted to investigate the effects of implementing a porous internal lattice structure with a thin outer shell on the articular contact mechanics of radial head hemiarthroplasty implants. The objectives of this study were outlined at the beginning of this thesis as follows:

1. To quantify the articular contact mechanics (*viz.* contact area and contact stress) of radial head hemiarthroplasty implants with a porous internal lattice structure and a thin outer shell using experimental methods;
2. To determine a critical porosity level of the internal lattice to optimize the articular contact mechanics of the hemiarthroplasty implant.

The hypothesis of this study, as given in **Chapter 1,** was that a porous internal lattice structure would reduce the effective stiffness of the implant, thus increasing hemiarthroplasty contact area and reducing contact stress relative to a solid implant.

4.2 Design and Development of a Radial Head Hemiarthroplasty with a Porous Internal Lattice Structure and a Thin Outer Shell

In **Chapter 2,** the design and development of a radial head hemiarthroplasty with a porous internal lattice structure and thin outer shell was outlined and discussed. A brief description of lattice structures, their build patterns and geometrical classifications were provided. Also discussed were the different types of unit cell structures that could be used to construct a lattice and the associated structural characteristics that have a significant influence on the resulting mechanical properties of a lattice. Finally, the fabrication of the radial head constructs was outlined for the use of experimental testing as conducted in **Chapter 3**.

Based on this review of prior research, a 4 mm^3 BCC unit cell was used to construct a uniform lattice within the geometric constraints of the Evolve Proline Radial Head System (Wright Medical) with a 0.5 mm uniform shell thickness. Three porous radial head implants were developed by modifying the internal strut diameter of the lattice. Strut sizes of 0.4 mm, 0.6 mm, and 0.9 mm were used corresponding to porosities of 80, 74, and 65%, respectively. The effective moduli of these radial head constructs were approximated using the Gibson and Ashby Model and the Nielsen Equation suggesting an 80 – 90% decrease in stiffness compared to a solid model of the same material and identical geometric parameters. SLS technology was used to additively manufacture the porous models using polyamide PA2200 (E = 1.64 GPa) and a solid model using UHMWPE (E = 0.69 GPa).

4.3 Effect of a Porous Internal Lattice Design on The Articular Contact Mechanics of Radial Head Hemiarthroplasty Implant

Chapter 3 presents a cadaveric study to test the radial head hemiarthroplasty implants designed and developed as in **Chapter 2**. The objective of this study was to determine if the articular contact mechanics (*viz.* contact area and stress) could be improved by implementing a porous internal lattice structure with a thin outer shell in hemiarthroplasty implants as compared to a solid implant. It was hypothesized that with increasing porosity, contact area would increase and contact stress would decrease on the premise of reduced implant stiffness provided by the internal lattice structure. Testing employed 11 cadaveric specimens in a testing rig under uniaxial compression and a flexion angle of 90-degrees. Preliminary investigations on the appropriate load magnitude to be used for testing suggested that articular contact mechanics reach a plateau around 150N and thus this magnitude of loading was employed herein. A subsequent preliminary investigation on viscoelasticity was performed to assess time dependent changes in articular contact mechanics over time. This revealed an increase in contact area and decrease in stress over time followed by a plateau between 4 – 6 minutes. As such, compressive testing of the radial head constructs was performed for a duration of 6 minutes. The contact area and stress were measured using a Tekscan sensor for three radial head hemiarthroplasty constructs with 80, 74, and 65% porosity, a solid hemiarthroplasty, and the native radial head.

The results of the study showed no significant improvement in contact area for the porous compared to the solid radial head implants. However, the radial head implants with a porous internal lattice structure demonstrated a significant decrease in contact stress with increasing porosity. Stress reduction at the joint interface can potentially reduce the rate at which cartilage wears over time which can be done by maximizing articulating contact area. However, this study suggests that a porous internal lattice structure can reduce contact stresses due to their impressive

energy absorbing capabilities despite no significant changes in contact area. The hypothesis of this section, with respect to contact stress, was shown to be supported.

4.4 Study Strengths and Limitations

The radial head hemiarthroplasty with a porous internal lattice structure and thin outer shell used in this thesis was designed and developed based on an extensive review of the literature. The work presented in **Chapter 2**, provide crucial insight into the mechanical properties and performance of lattice structures allowing for a comprehensive investigation to be performed in the **Chapter 3**. The uniform BCC lattice design used is one of the most recognized lattice constructs amongst previous academic work thus, the findings presented in this thesis may be easily translated to future work using different or more complex lattice designs. This study involved two preliminary investigations on the appropriate load magnitude for testing and the potential for changes to occur over time due to the viscoelastic properties of cartilage. This data should prove useful to other investigators performing similar work in the future.

A limitation to the cadaveric study is the complexity associated with additively manufacturing lattice geometries. SLS has been successful in generating complex lattice geometries however literature on implementing a porous internal lattice structure in an enclosed design space as done in the presented study is scarce. The 3D printed structures appeared to have no visible defects or broken cells and a direct light source revealed distant internal lattice structures. Still, insufficient removal of excess powder and unwanted fusion of powder particles in the pores of the lattice or against the implant walls may have occurred. Thus, a more refined method of analysis such as computer tomography (CT) may be necessary to validate successful fabrication of the porous structures. Another limitation was the use of fresh-frozen cadavers which may have altered the material properties of the cartilage though effects have been shown to be modest if any.

4.5 Future Studies

Future work should include experimental or computational investigations to evaluate the effective stiffness of the proposed radial head models which can be compared to the moduli approximated by theoretical model such as the Gibson and Ashby model and the Nielsen Equation. Investigations on the effective strength of the radial head implants with porous internal lattice structures may be conducted to ensure they can withstand a wide range of possible physiologic loading conditions without failure to the internal struts or outer shell. This radial head design should also be assessed with other materials to determine if the results can be translated to high-modulus materials that have been approved for implantation (*i.e.* CoCr, PyC). Future cadaveric studies should also evaluate if the improvements seen in the contact stress of the proposed implants produce less cartilage wear as expected.

4.2 Conclusion

A porous internal lattice structure with a thin articular wall may be able to improve articular contact mechanics in hemiarthroplasty implants thereby reducing cartilage wear. The work presented in this thesis suggests that a structural lattice design can lower the effective stiffness of an implant, such that with increasing porosity (decreasing internal strut diameter) increased contact area and decreased contact stress. The results of the cadaveric study did not reach significance in contact area though significance was achieved with respect to mean and maximum contact stress which decreased by approximately 40 – 60% with the introduction of a porous internal lattice structure compared to the solid model. The presented work also investigated an appropriate load magnitude for experimental testing (150N) and highlighted the importance of considering viscoelasticity in future experimental and computational investigations.

Further research is required to elucidate the effects of a porous internal lattice structure on preserving the integrity of the opposing cartilage in hemiarthroplasty implants. These developments would allow for the optimization of commercial radial head devices and other hemiarthroplasty implants, reducing the likelihood of suffering from pain and stiffness after these procedures. The present study is the first to investigate the concept of hemiarthroplasties with a porous core and suggests potential significant advantages with these new design approaches.

Curriculum Vitae

Name:	Jessica Benitah
Post-secondary Education and Degrees:	The University of Western Ontario London, Ontario, Canada 2015 – 2020 B.A. The University of Western Ontario London, Ontario, Canada 2020 – 2022 M.A. Candidate
Honours and Awards:	Western Scholarship of Excellence 2015 – 2016 Deans Honours List 2017 – 202
Related Work Experience	Teaching Assistant The University of Western Ontario 2020 – 2022 Western Engineering Research Student The University of Western Ontario 2019 – 2020

Conference Presentations:

"Effect of a Porous Internal Lattice Design on Hemiarthroplasty Implant Articular Contact Mechanics"
Podium presentation at the 2021 Annual Meeting of the Canadian Orthopaedic Association/Canadian Orthopaedic Research Society for orthopaedic innovation.

"The Viscoelastic Properties of Articular Cartilage Affect the Contact Mechanics of Both Native and Hemiarthroplasty Articulations"
Poster presentation at the 2022 Annual Meeting of the Canadian Orthopaedic Association/Canadian Orthopaedic Research Society for orthopaedic innovation.